MASTER THESIS

Development of a multimodal anthropomorphic liver phantom for the improvement of navigated tumour treatment

H.C. Ruitenbeek

Department of Technical Medicine
University of Twente

Department of Surgery
Antoni van Leeuwenhoek

EXAMINATION COMMITTEE
Medical supervisor & Chairman: Prof. dr. T.J.M. Ruers
Technical supervisor university; ir. E.E.G. Hekman
Technical supervisor institution: dr. M.F. Fusaglia
Process supervisor: B.J.C.C. Sweep, MSc.
External Member: B. Wermelink, MSc.

A thesis submitted to the University of Twente for the degree of

Master of Science in Technical Medicine

ANTONI VAN LEEUWENHOEK
NEDERLANDS KANKER INSTITUUT

UNIVERSITY OF TWENTE.

Acknowledgements

During this graduation I have worked on a challenging project and have had all the freedom to do so in my own way. Prof. dr. Theo Ruers supervised me and granted me all the space I needed. He also provided his critical notes that kept me focused on the clinical relevance and implementation of the project.

Daily guidance on my project was given by dr. Matteo Fusaglia who has always been of great support and empowered my work with his confidence throughout the year. Our weekly meetings have inspired me more than once and cooperation has always been very enjoyable and relaxed.

I was supported on every aspect of my graduation by Jasper Smit, MSc. By always being approachable and guiding me with the tremendous effort he helped me during long days of work and also guided me excellently in the clinical part of the graduation, for which I thank him a lot.

My sincere thanks to ir. Edsko Hekman who introduced me to the process of product design and phantom development. His guidance as technical supervisor helped me with a structured way of addressing the project and taught me how to get back on track.

I am particularly grateful for all the help and advice given by Bregje Hessink-Sweep, MSc., on personal development throughout my last two master years. During intervisions you were always understanding and helped me become aware of the challenges I had to face but also of the progress I had already made.

In general, the Antoni van Leeuwenhoek hospital has been a great place to work. Everybody that I've encountered was very helpful and interested in my work.

Finally, my graduation would not have been the same without all my happy colleagues from the surgery department. Everybody has cheered me up, is great fun to work with and good company for Friday afternoons.

Huib Ruitenbeek

Amsterdam
11 December 2019

Abstract

In liver surgery, new technologies and equipment are introduced to aid the surgeon in finding diagnosed lesions and achieving successful resection. To support the development of surgical navigation technologies and provide a simulation setting for researchers and surgeons, a multimodal, patient-specific liver phantom needs to be developed. The phantom needs to consist of substitute structures for parenchyma, vasculature and tumours. The geometry should be patient-specific which means the size and outline of the liver, together with vasculature and lesions, are based on human anatomy and resemble a specific case. First, material selection was performed to select the substitute materials to build the phantom. Criteria where realistic ultrasound contrast of parenchyma, vasculature and tumours. For MRI the contrast must be sufficient for vasculature and tumour segmentation to create a 3D model, using the same method as in patient scans. Candle gel was found to be the best material to create a realistic ultrasound aspect of liver parenchyma based on intensity differences and mechanical properties. For vasculature, cavities filled with water show the best resemblance to human liver vasculature. The hollow vasculature was created by extracting a 3D printed vasculature model after casting the candle gel. The combination of candle gel parenchyma and hollow vasculature can clearly be distinguished on MRI and therefore can produce a 3D model similar to a preoperative model used in surgery. Tumours consist of a mixture of candle gel and carnauba wax to realize ultrasound and MRI contrast with the parenchyma substitute. Finally, a patient-specific-liver phantom was created with the selected materials and validated by comparison to the patient model it was based on. The parenchyma was shaped using a 3D printed mold of the liver outline. In this mold the 3D printed vasculature model together with the tumour were placed. The candle gel was poured into the sealed mold to realize the phantom. The phantom shows high geometrical resemblance with a volume difference of 66 cm^3 and a 95-percentile Hausdorff distance of 5.7 mm. The hepatic and portal vasculature show corresponding bifurcations. Practical use of the phantom shows that it is useful for performing US to MRI registrations and use of ultrasound guided ablation equipment. Successful positioning of tumours was not achieved and the phantom is very fragile. Challenges to be overcome in future research are accomplishing accurate tumour placement and applying a protective element to enlarge the durability of the phantom.

Contents

List of Figures

List of Tables

1. General introduction and Background

Primary liver cancer is diagnosed in 800 patients each year in the Netherlands.[1] Hepatocellular carcinoma (HCC) is the most common primary liver cancer with 90 percent of the cases. Furthermore, HCC is the third-most common cause of cancer related deaths worldwide.[2] Factors such as liver cirrhosis and hepatitis increase the risk of developing HCC.[3] Moreover, most liver lesions are metastases originating from colorectal cancer (CRC). In 2018 approximately 14.000 patients were diagnosed with CRC in the Netherlands.[1] Approximately half of all patients with CRC will develop liver metastases.[4]–[8] In 30-70 percent of the cases liver metastases will develop in patients with advanced CRC of which 25 percent have metastases at presentation.[9] Liver metastases cause two thirds of the deaths in CRC patients.[8] Treatment options are radiotherapy, chemotherapy, surgery or a combination of these. Other common primary tumour sites that metastasize to the liver are the pancreas and breasts, but virtually any tumour can metastasize to the liver.[10]

1.1 Clinical Background

Lesions can be localized in every segment of the liver and in all sizes. Resection of liver lesions is still the best option for treatment.[8]–[10] However, resection is only feasible in 20 to 30 percent of the cases because of extrahepatic disease or the anatomical distribution of the disease.[14]–[16] Studies show that up to 80 percent of the liver can be resected with an operative mortality of less than 5 percent, if the residual liver parenchyma is healthy and disease free.[17]–[19] Surgical resection can be done in two ways: Anatomical resection aims at removing segments of the liver along the anatomical planes as defined by Couinaud [20] (Figure 1). Single or multiple segments can be resected individually or, when a hemi hepatectomy is performed, the right (segments V, VI, VII and VIII) or left (segments II, III, and IV) liver lobe is removed at once. A different way of removing liver lesions is by wedge resection, focusing on removing a small volume of the liver containing the lesions. Wedge resection is reported to have a higher risk of positive resection margins.[21] However, for single rather than multiple lesions, the incidence of positive resection margins and the five-year survival is equivalent for both wedge resection and segmental resection.[22]

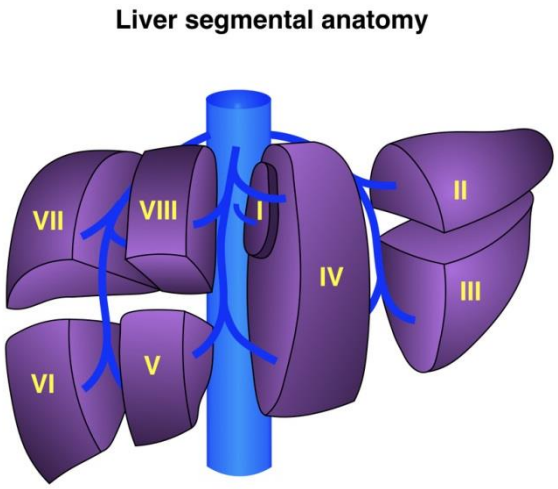

Figure 1: Liver segments as defined by Couinaud.[20] **Image copied from Radiopaedia.org**[23]

If resection of all lesions is not feasible, unresectable lesions can be treated using ablation techniques. Radiofrequent ablation (RFA) uses a high frequency alternating current to heat the tumour tissue leading to thermal coagulation. Under ultrasound imaging, a gradually enlarging eclipse can be seen indicating the coagulated tissue.[24] Microwave ablation (MWA) is another ablation technique used to treat liver lesions, introduced in 1979 by Tabuse.[25] Microwave energy penetrates several centimeters into the tissue and is absorbed to be transferred to heat. In contrast to RFA, MWA does not rely on conduction of heat for the coagulation of tissue. Both techniques can be used to treat liver malignancies of colorectal origin with MWA showing less ablation site recurrences.[26] The limitations in the use of RFA and other locally ablative modalities are the size of the tumour and its location close to major biliary or vascular structures.[27]

Besides surgery and ablation, another treatment option is neoadjuvant and conversion chemotherapy. Neoadjuvant chemotherapy refers to the administration of preoperative chemotherapy for initially resectable colorectal liver metastases (CRLM). Patients with initially unresectable CRLM receive conversion chemotherapy in an attempt to convert to resectability. Response rates for conversion chemotherapy are approximately 50 percent, with up to 20 percent proceeding to liver resection with curative intent.[28]–[32] Along with response to chemotherapy comes the problem of 'vanishing' or 'disappearing' lesions. This refers to complete response or disappearance of a liver metastasis on cross-sectional imaging after preoperative chemotherapy. Vanishing lesions occur in 5 to 25 percent of patients who undergo preoperative systemic therapy, and varies depending on the quality and type of cross-sectional imaging.[33], [34] Intraoperatively, approximately half of the vanishing lesions can be found by systematic ultrasound exploration of the liver [35] and residual macroscopic disease at the vanishing lesion site can be expected in about 25 to 45 percent of patients.[33], [36], [37] Accurate localization of the vanishing lesion sites or navigation towards them can thus be important for patient outcome.

The wide variety in CRLM and the above discussed treatment options complicate liver surgery and explain the demand for new technologies to support decision making and treatment. Detailed knowledge of the patient-specific hepatic and portal vasculature as well as lesion localization intraoperatively contribute to successful surgical resection and higher preservation of functional liver tissue.[38]–[40]

1.2 Technical background

During liver surgery, diagnosed lesions are to be found using palpation and ultrasound imaging. During laparoscopic procedures it becomes even harder to localize these lesions as palpation is not an option. Preoperative scans and three dimensional (3D) models are used to assist in finding these lesions intraoperatively. The pre-operative scans and 3D models show the location of hepatic lesions in relation to anatomical structures such as the gall bladder, hepatic vascularity and bile ducts. Nevertheless, some lesions remain hard to find through palpation, and localization by means of intraoperative ultrasound can be time consuming. In the NKI-AvL, the surgeon is often provided with a preoperative 3D model, visualizing patient-specific vasculature and lesions based on a preoperative contrast-enhanced, magnetic resonance imaging (MRI) scan.

This 3D model is based on a diagnostic MRI or computed tomography (CT) scan and contains the liver outline, part of the vena cava, hepatic vein, portal vein, diagnosed lesions and gall bladder with bile ducts. These structures are "segmented" which means they are delineated on each image slice, if

these delineations are stacked on top of each other they form a three-dimensional representation. Figure 2 shows an example of a 3D model as it is used during surgery.

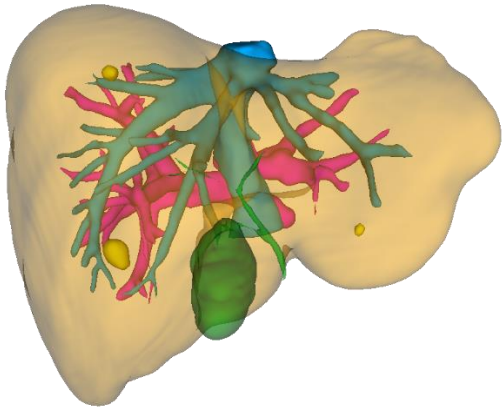

Figure 2: Example of a 3D model as it is used during surgery. The hepatic vein is pictured in blue, the portal vein in purple, three lesions in yellow and the gallbladder in green.

As additional support to the surgeon, the display of this 3D model, together with the intraoperative instrument position is in use and surgical navigation systems are being developed. Development of these surgical navigation systems is usually performed in studies that require *in vivo* testing. This intraoperative research is limited by the amount of procedures and the possibilities of performing developmental work during them varies. The development of a realistic simulation setting would therefore support the development of surgical navigation systems. This testbed simulates the preoperative and intraoperative environment in terms of image acquisition. Ultrasound and MR scans of a phantom can be used as data to develop and test image registration and tumour localization as would be performed intraoperatively.

Intraoperative ultrasound

During liver surgery, intraoperative ultrasound (IOUS) is used to locate the diagnosed metastases and scanning the liver for additional lesions.[41] Lesions have usually been imaged using CT or MRI. When using IOUS the location of the lesions is approached by following structures such as the hepatic and portal vein branches. Once the lesion is found, IOUS is also used to determine resection planes. By imaging the tumour borders and surrounding vasculature a resection plane can be determined from the position of the probe. If RFA/MWA ablation is intended, IOUS is used to localize the lesions and guide the needle to the correct position.

Liver lesions can have different appearances on US, even within one patient. A hypoechoic halo is often seen around metastases and HCC but also around adenomas, focal nodular hyperplasia's and hemangiomas.[42] The cause is controversial. Possible causes are pressure atrophy of the hepatocytes, leaving sinusoidal blood vessels that are imaged as the halo.[43] Another explanation is that the halo shows proliferating tumour cells.[44] Malignant lesions can show virtually any kind of sonographic pattern such as echogenic, echo poor and acoustic shadowing from calcified metastases.[42]

In general, it can be stated that dense materials reflect sound and soft materials let the ultrasound waves transmit. The images produced on the ultrasound machine are the reflections that occur on the transitions of materials with different acoustic impedance. The acoustic impedance is the product of the density and sound propagation velocity in a medium.[45] For intraoperative ultrasound this means that liver parenchyma shows dense speckle, resulting from the numerous transitions between cell

structures in the hepatic lobules. Vasculature is imaged as almost anechoic but portal veins can be distinguished by a hyperechoic layer, caused by Glisson's capsule.

Liver phantoms

Different available commercial phantoms can be used for ultrasound training. A number of phantoms are suitable for ultrasound imaging of the liver. Four examples are presented in Figure 3. The Triple Modality 3D Abdominal Phantom (CIRS Inc., Norfolk, VA, USA) provides a training model for ultrasound guided needle insertion and navigation technology. The phantom contains parts of the liver, vascular structures and liver lesions. The CIRS phantom allows for multimodal medical imaging (US, CT and MR). Another commercial liver phantom is the IOUSFAN (Kyoto Kagaku Co., Ltd, Kyoto, Japan). This phantom is designed as a practice and demonstration tool for abdominal intraoperative ultrasound procedures. In contrast to the CIRS phantom, the IOUSFAN has a realistic appearance and it can be used for laparoscopic ultrasound. Syndaver is a company that produces highly realistic canine and human phantoms from water, fiber and salt but use in literature has not been described yet. Finally, the FAST Exam phantom (CAE Healthcare) consists of an entire torso intended to train a percutaneous ultrasound examination procedure. This FAST exam phantom lacks pathology.

The downsides of these phantoms are the lack of patient-specific pathology, high costs and the fact that they don't survive destructive procedures such as biopsies or ablations. Moreover, the anatomy is based on basic or average anatomy. Specific cases of tumour orientation or atypical vasculature cannot be recreated using these phantoms. Storage of these phantoms is another drawback as microbial growth and dehydration are a hazard for all of these phantoms.[46]

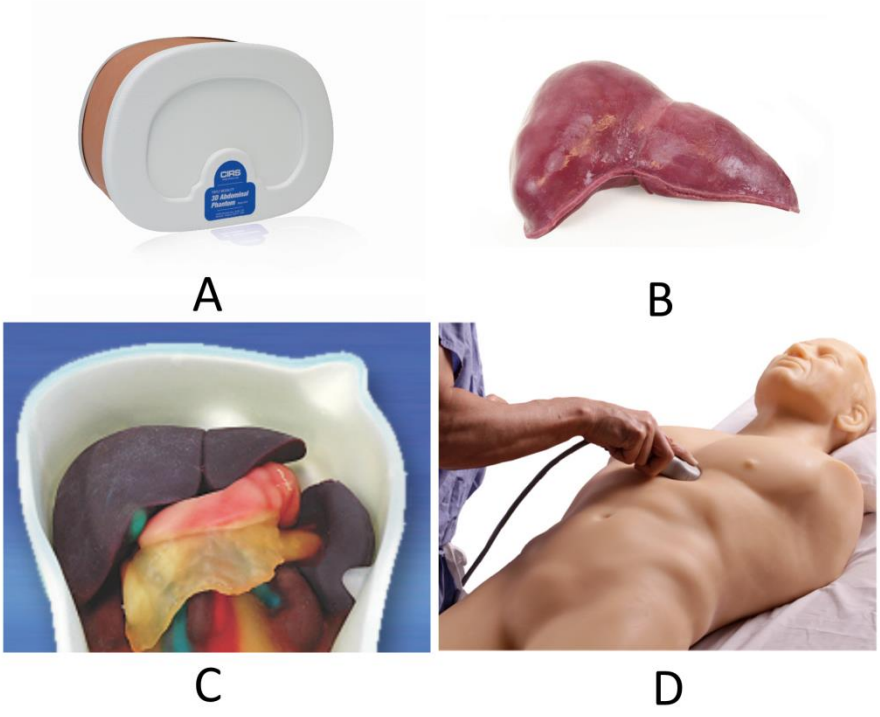

Figure 3: Commercially available ultrasound phantoms. A: Triple modality phantom (CIRS Inc.), B: Liver phantom (Syndaver), C: IOUSFAN phantom (Kyoto Kagaku Co.,Ltd), D: FAST Exam phantom (CAE healthcare)

1.3 Problem definition

Finding hepatic lesions during surgery remains difficult, especially in laparoscopic procedures where hidden lesions cannot be localized through palpation. Intraoperative ultrasound combined with surgical navigation can assist the surgeon in orientation. Ultrasound image quality is inferior compared to CT or MRI and US based navigation is still in development. As a result, the time that is needed during surgery to localize lesions can be extensive. Surgical navigation systems can shorten this time and help in achieving negative resection margins, meaning no tumour cells are found by the pathologist within a specified distance from the resection edge. This results in extensive developmental research and in a steep learning curve to using surgical navigation during OR. Development of surgical navigation techniques using ultrasound requires significant testing. This testing currently involves obtaining US images from volunteers or patients and practicing of the navigation workflow during liver surgery. Only a maximum of 15 minutes operating time is devoted to this development in a single operation to minimize patient burden and delay. Also, before images can be acquired, permission of all participants is needed and, depending on the experiment, METC approval may need to be acquired. All in all, the small amount of time available to simultaneously develop surgical navigation systems and practice the workflow inhibit rapid progression of the technology and delays implementation.

1.4 Objective

Radical resection, ablation treatment and tracing vanishing lesions all benefit from the development of surgical navigation techniques and therefore profit from the development of a liver phantom to be used as a simulation setting. Studies show that simulation settings and practicing environments are beneficial for the outcome of performing novel medical procedures and can help to introduce them into the operating theatre.[47], [48] The objective is to aid the development of surgical navigation systems by building a development and simulation environment of image-guided liver surgery. For research purposes, the imaging characteristics are the most important. For the surgeons, trying out new navigation applications on the phantom gives them a chance to get a hands-on in a risk-free environment.

1.4.1 Requirements

To achieve the objective of realizing a development environment and simulation environment simultaneously a list of requirements is composed. First, the phantom should mimic US imaging of a human liver and probe-phantom interaction should feel the same as probe-liver interaction. This enables a surgeon to train on using intraoperative US in the most optimal way and means that biomechanical properties such as elasticity and stiffness of the phantom should approach the ones of liver tissues. Furthermore, the shape of the anatomical structures should be reproduced such that US views are identical to intraoperative situations. Second, to contribute to the development of US navigation techniques the phantom should be suitable for MRI or CT imaging. US to MRI/CT registration is required to be able to relate the preoperative imaging to the intraoperative situation and thereby performing image-guided surgery. On CT or MR imaging, contrast has to mimic the contrast levels found *in vivo* between parenchyma, vasculature and tumours. Sufficient contrast levels will allow segmentation of these structures and the creation of a 3D model. Finally, the phantom should be patient-specific, meaning that it’s possible to simulate a specific patient case or create custom anatomy.

List of requirements

This list of requirements describes what is needed for a good solution to the problem. If one of these requirements is not met, the product fails.

- Use requirements:
  - The product should have realistic US, CT and MRI image properties.
  - The product can be used with conventional imaging devices.
  - The product can be used for surgical actions such as incisions, needle insertions and ablation.
  - The mechanical properties of the phantom must be close to real tissue, to simulate haptic feedback.
- Safety requirements:
  - The product should not be toxic for users or producers
  - The product should not damage the used medical equipment, e.g. ultrasound probes.
- Functional requirements:
  - The product should contain liver parenchyma, vascularity and tumours.
  - The product should be patient-specific, meaning position of the mentioned anatomy must be in correspondence with the imaging it is derived from (preoperative CT or MRI).
- Space requirements:
  - The product should be 1:1 in size and volume compared to patient.
- Time requirements:
  - The product must be producible within 2 weeks
  - The product should be stable for several weeks at room temperature or in a cooled environment (7°C)
- Use wishes:
  - Production is not complicated and doesn't consume too much time.
  - Total costs per phantom are less than 500 euros.
  - It must be possible to use the product without protective gear.
  - Components are recyclable.
  - Parenchyma is transparent for training purposes.

1.5 Thesis outline

The outline of this thesis is schematically illustrated in Figure 4. In Chapter 1 the relevance of this project together with the research aim has been explained. Chapter 2 describes a sequence of sample experiments that were performed to select the materials for each component and production methods of creating a liver phantom. The resulting materials and production methods were used to build a patient specific, multimodal phantom, this process is described in Chapter 3. In Chapter 4 the results and challenges found in this study are discussed. The thesis is concluded in Chapter 5. Finally, in Chapter 6, possible solutions to the remaining challenges in the development of the phantom are discussed.

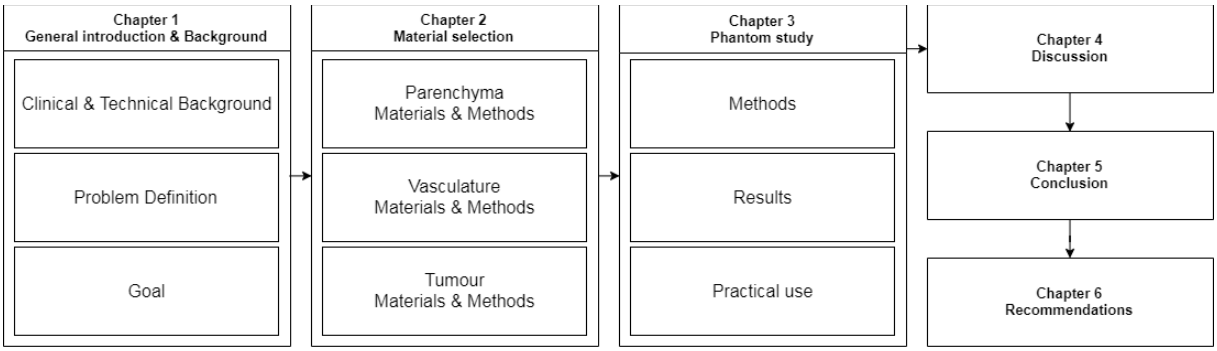

Figure 4: Thesis outline

2. Material selection

The first step in the development of a multimodal phantom is material selections. Diligent material selection is crucial since it will influence the functioning, the form, the durability and the expense of the phantom. The requirements presented in paragraph 1.4.1 are used as point of view during the literature study. In order to produce a functioning phantom the materials have to meet the imaging requirements, physical requirements and have to be practically producible within the facility. The phantom consists of parenchyma substitute, vasculature and tumour tissue. The challenge is to find a combination of materials for these three structures that meets the set requirements in multiple imaging modalities. The phantom should produce ultrasound images similar to a human liver, have sufficient image characteristics on MRI to segment vessels and lesions easily and have mechanical properties comparable to a human liver to simulate intraoperative probe manipulation. Literature study has been performed to make a first selection of materials that have been used to produce phantoms for medical imaging or training. Ultimately a selection of materials is tested on imaging performance and practicality. The results of these tests lead to a final selection of materials and methods for the phantom presented in Chapter 3. The material selection for the three structures and methods of production are presented in this chapter.

2.1 Parenchyma

To create a selection of potential materials to use as parenchyma, a literature study on phantom materials and liver phantoms in particular was performed. Culjat *et al.* [49] describes a review of tissue substitutes for US imaging. The benefits and disadvantages of US mimicking materials that have been used over the past decades are discussed.

The following items are at stake in the selection of parenchyma substitute material;

Acoustic impedance: The acoustic impedance of a medium is the product of the density and sound propagation velocity in a medium [45] and is important for the ultrasound imaging performance. Clinical ultrasound scanners are calibrated using the speed of sound in soft tissue. Using a parenchyma material that has a different speed of sound results in a deformed image and incorrect distance measurements on the ultrasound machine.

Biomechanical similarity: The Young's modulus is taken into account to give an indication of biomechanical similarity to real liver parenchyma.

Practicality: Processing of the material should not require advanced conditions or tools. Aspects that are in favor are; fabrication at room temperature, non-toxicity and reusability. Additionally, the material should be easy to obtain and fairly cheap. Also, the fabrication method should be relatively easy to execute as this phantom is being developed in a short time and in a research setting

In terms of MRI imaging characteristics, different MRI sequences can be used in the search for sufficient image contrast. Also, echo time can be adjusted to increase contrast if necessary. Therefore only materials that perform well on ultrasound and that are usable in terms of practicality will be imaged using MRI.

2.1.1 Material candidates

Candle Gel

Candle gel, or paraffin gel, is a material used to create clear decorative candles. It is a mix of usually 95% paraffin oil and 5% thermoplastic resin although slightly different concentrations are sometimes used to create different density types. Vieira *et al*. [50] used it to create a breast phantom and Shevchenko *et al.* [51] used it to create a multimodal liver phantom for testing of surgical navigation systems. Its melting point is 68˚C and it is relatively cheap. Besides, it has a speed of sound of 1425 – 1432 m/s where human liver parenchyma is estimated at 1540 m/s. Its main disadvantage is the forming of air bubbles but this can be overcome by placing the molten gel in a vacuum chamber before use.

Hydrogels

Two similar materials that can be used are gelatin-based and agarose gel-based materials. These substances are both easy to use and are mixed with graphite powders to obtain realistic US speckle. Also, with a reported sound velocity of 1498-1600 m/s for agarose and 1520 – 1650 m/s for gelatin both materials could be suitable to produce a realistic phantom in terms of speed of sound. Both materials, however, are vulnerable for microbial invasion. Additionally, a major drawback of these materials is its limited lifespan of a number of weeks when stored refrigerated. Zell *et al.* [52] have reviewed hydrogel material based on agarose and concluded it suitable for quick and easy preparation. However, the study also confirms the low durability.

Polyurethane

Polyurethane gel has acceptable acoustic properties for soft tissue mimicking although not as similar to liver parenchyma as the aforementioned hydrogels. The elastic recovery, immunity from microbial invasion [53] and high durability could make it a good material for a long lasting phantom. The phantom described by Rethy *et al.* [54] has polyurethane as base material for liver parenchyma. The sound velocity in this polyurethane was measured 1425 m/s,.

Polyvinyl alcohol

Polyvinyl alcohol-based materials (PVA) show good acoustic properties that can be adjusted during the preparation process.[55] This preparation process is also the downside of using this material since the production of a PVA phantom requires multiple freeze-thaw cycles taking up to 24 hours. A sound velocity of 1520 – 1610 m/s is close to human liver tissue. However, the material characteristics are affected by the execution of the freeze-thaw cycles that are prone to mistakes.

Silicone

Silicone polymer-based materials have good durability, variable elasticity and can be mixed with (graphite) powders for realistic US speckle. The drawback however is the low speed of sound compared to liver parenchyma.[49] Additives can be used to adjust the properties of silicone and increase echogenicity and speed of sound, or to lower the Young's modulus [56], [57] Pacioni *et al.* [58] describes the fabrication of a patient-specific ultrasound liver phantom. In the study, the silicone is used as base material for both parenchyma and tumours. Graphite powder is added to achieve realistic ultrasound characteristics. One of the reasons silicone was used is that the created phantom should last for many years. A drawback of using silicone is the image distortion as a result of a different speed of sound in the material compared to real human liver parenchyma (1080 m/s versus 1540 m/s respectively). The authors used the phantom in a hybrid simulator and could solve this problem by software manipulation.

Other

Magnesium silicate-based tissue substitutes have good acoustical properties but are not self-supportive so cannot be formed or molded into predefined shapes. Ethylene glycol based materials are not suitable for soft tissue mimicking because of their high speed of sound, density and low attenuation. [49]

Table 1 and Table 2 give an overview of the material properties. Based on the literature study four materials are selected for sample testing. The most important aspect is density and sound propagation velocity as these are related to both imaging properties and mechanical properties.

Table 1: Acoustical properties of the analyzed materials.

Material	Sound velocity (m/s)	Density (kg m^{-3})	Attenuation coefficient (dB cm^{-1} Mhz^{-1})	Source
Liver	1595	1060	0.5	ICRU
Agarose	1498 - 1600+	1016-1100	0.04-1.40	Burlew *et al*.[59]
Candle Gel	1425(MDT), 1432(HDT)	810(MDT), 840(HDT)	0.32-2.04*	Vieira *et al*.[50]
Gelatin	1520-1650	1050	0.12-1.5	Burlew *et a*l.[59], Bush *et al*. [60]
Plastisol	1379	1000	0,63	de Carvalho *et al*.[61], Spirou *et al*.[62]
Polyurethane	1425-1468	1130	0.13	Rethy *et al*.[54], Kondo *et al*.[53]
PVA	1520-1610	1030-1070	0.04-0.35 0.08-0.22	Kharine *et al*.[55], Surry *et al*.[63]
Silicone	1080	1080	1.5	Pacioni *et al*.[58]

*Dependent on amount of carnauba wax

Table 2: Young's modulus, processing temperature and relevant properties of the analyzed materials

Material	Youngs modulus (kPa)	Temperature	Pros	Cons
Liver	20-60 [64]	n/a	n/a	n/a
Agarose	7.6-195 [65]	Room temperature	Adjustable imaging properties	Short durability, bacterial invasion
Candle Gel	15-18(MDT),30-34(HDT) [50]	75°C [66], 61-82°C [50]	Cheap, easy to work with, reusable	Fragile, air bubbles
Gelatin	4.8-158 [65]	Room temperature	Adjustable imaging properties	Short durability, bacterial invasion
Plastisol	3-200 [67] 0.1-100 [68]	180°C [61]	Reusable, decent suitability proven	High working temperature, fumes
Polyurethane	5-63.6 MPa [69]	Room temperature [70]	No equipment needed	Not reusable
PVA	20-600 [71]	freeze thaw cycles [63]	Adjustable imaging properties	Very impractical
Silicone	50 [58]	Room temperature [72]	Easy to work with	Not reusable

MDT=Medium density type
HDT=High density type

Compared to a human liver, agarose, gelatin and PVA may have an equal sound velocity. Silicone (without additives) has the largest deviation. In terms of density, gelatin and silicone have and equal density compared to human liver parenchyma, candle gel has the largest deviation with approximately 200 kg/m^3. The attenuation coefficient of agarose, candle gel and gelatin can be equal to liver parenchyma. However, they also have a wide range of measured attenuation coefficient. Silicone has the largest deviation.

Considering the fact that the phantom should be durable, agarose and gelatin can be dismissed. A maximum stability of several weeks is too short and the vulnerability for bacterial invasion is not desired. Candle gel does not score the best on sound velocity and density but has a melting temperature that is easy to work with and the gel is reusable. Plastisol has been used in breast phantoms before and is reusable. Its downside is the high working temperature and the toxic fumes produced during melting. PVA has adjustable imaging properties that resemble soft tissue well. However, in a later phase where the phantom needs to be molded to mimic patient-specific anatomy the preparation process of PVA is a problem. Finally, silicone and polyurethane are two more expensive materials that have the benefit of vulcanization at room temperature. These materials are also found in commercial phantoms and are used to mimic human tissue in special effects industry. Its imaging properties however may be hard to tweak and once hardened, the material is not reusable.

Concluding, four materials will be tested; candle gel, plastisol, polyurethane and silicone.

2.1.2 **Selection methods**

A small, simple phantom of each of the four materials was created to test on imaging performance. The phantom has a triangular shape and contains models of a vessel and tumour. To create this phantom a vessel and a tumour substitute are positioned in a mold. Then the parenchyma substitute is poured to embed the vessel and tumour. As a vessel substitute, consumer grade silicone is used. As tumour substitute, a different material combination is used for each phantom, derived from the performed literature study.

The basic phantom design is illustrated in Figure 5. A triangular shape was created by placing a glass jar in an angle while pouring the parenchyma materials. The embedded structures can be imaged from different angles, changing the orientation of the structures in the image plane. This can be important in US imaging, where signal from deeper structures is influenced by material above.

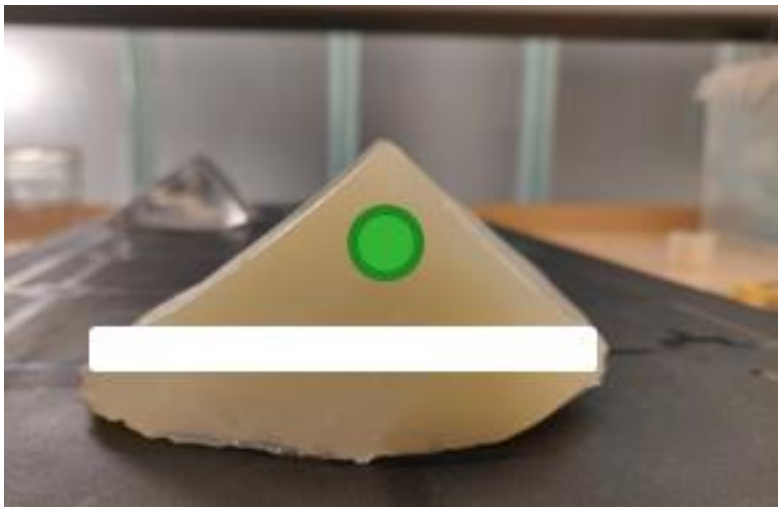

Figure 5: Basic design of small phantom for material tests. The white line resembles the straight vessel that is placed in each phantom. The green circle indicates the position of the embedded tumour.

For vessel creation during sample testing, conventional bathroom silicone is chosen in all samples. It can withstand temperatures up to 180°C which is needed when used in combination with plastisol. Apart from that, it has been used in earlier phantom tests in the hospital where it had anechoic aspect on US, which is comparable to real vessels. Its properties in CT and MRI are acceptable in combination with plastisol as they offer enough contrast with the parenchyma. The contrast with other phantom materials will be reviewed during the sample testing.

Small tumours were created for each small phantom. Spheres with 1.5 cm diameter were created using a simple spherical mold. Carnauba wax was added to candle gel following Vieira *et al.*[50] In plastisol a tumour was created by excluding plasticizer from the mixture. In silicone the method of Pacioni *et al.*[58] was followed. In polyurethane, candle gel with added carnauba wax was used as tumour. The composition of the small phantoms can be found in Table 3.

Candle gel

Candle gel was melted in a water bath at a temperature of 90°C. Two teaspoons of magnesium oxide were mixed in. After 5 minutes of mechanical stirring the candle gel was placed in a vacuum chamber for 5 minutes to prevent air bubbles at -84 kPa or -630 mmHg. A shallow layer was poured and allowed to cool down. The tumour and vessel were placed on top and the rest of the candle gel was poured around them.

Plastisol

The supersoft plastic and softener were mixed and heated in a pan until the mixture turned thick. Heating continued until the mixture turned back into a pourable state and had a temperature of around 170°C. A shallow layer was poured. A tumour was placed on top after a while and a new layer was poured around. After the second layer had cooled the vessel was placed on top and the remaining mixture was poured. The phantom was allowed to cool overnight.

Silicone

The method of creating the silicone sample is based on the method of Pacioni *et al.* [58] Ingredients were mixed by ratio of weight with silicone part A. Then, silicone part B was mixed in and the mixture was stirred thoroughly for around 2 minutes. The compound was then placed in the vacuum chamber and degassed at -84 kPa or -630 mmHg for 5 minutes. The jar was prepared by fixating the

tumour and vessel with wire. After degassing the mixture was poured into the jar and left to cure overnight.

Polyurethane

Part A and B of the polyurethane were mixed and thoroughly stirred for 3 minutes. The mixture was also degassed at -84 kPa or -630 mmHg for 5 minutes. The tumour and vessel were fixated in the jar with wire. The polyurethane mixture was poured into the jar and needed 24 hours to cure.

Table 3: Final composition of sample phantoms that were used in parenchyma material selection.

Phantom	Parenchyma material	Tumour material
Candle Gel	Candle Gel MgO_2 1g/100mL	Candle Gel MgO_2 1g/500mL
Plastisol	Plastisol 66% Plasticizer 33%	Plastisol 100%
Silicone	Ecoflex 00-10 (Silicone) 53% Graphite 5% Thinner 15% Slacker 7% Vaseline oil 20%	Ecoflex 00-10 (Silicone) 88% Graphite 2% Vaseline oil 10%
Polyurethane	Polyurethane 2/3 So-Flex II 1/3	Polyurethane 2/3 So-Flex II 1/3 MgO_2 1g/500mL

The small phantoms will be evaluated by ultrasound and MRI imaging, as well as tactile aspect.

Ultrasound

Ultrasound images of all samples have been acquired on a BK Medical, BK5000 intraoperative ultrasound system (BK Medical, Herlev, Denmark) in combination with the T-shaped intraoperative probe at 7.5 MHz using the protocol that is clinically used during intraoperative ultrasound for liver surgery. Images have been acquired from multiple angles to study image characteristics of the phantom in different formations. The images were exported in DICOM format.

MRI

All samples were scanned using a T2-weighted protocol clinically used for breast imaging in a Philips Ingenia 3.0T MRI scanner (Philips Health Care, Best, the Netherlands).

Table 4: MRI settings used for scanning the small phantoms

Acquisition type	3D T2
Acquisition matrix	200x200
Magnetic field strength	3T
Pixel spacing	0,625mm
Slice Thickness	2mm
Slice distance	1mm
Echo time	176ms
Repetition time	1250ms

All images were exported in DICOM format. The contrast between the lesion and parenchyma, and between the vessel and parenchyma were again determined by an intensity profile and comparing the mean pixel value.

2.1.3 Selection results

Ultrasound

Figure 6 shows ultrasound images of the samples. In all images the parenchyma, a vessel and a tumour are visible.

On ultrasound images the candle gel has diffuse speckle and penetration depth is approximately 6cm. Plastisol shows aspect similar to candle gel, but the speckle in the plastisol is more heterogeneous. The contrast with the vessel is sufficient but the vessel causes significant reflections. For instance, a difference compared to candle gel is that the parenchyma behind the vessel in plastisol is not imaged clear and shows different aspect compared to candle gel. In silicone only 2-3cm of the material can be imaged which shows as a hyperechoic band with dense speckle where the tumour and vessel are visible only when the probe is pressed into the phantom so that the vessel or tumour falls within the imaging range. No reflections can be seen deeper into the phantom. In polyurethane, vessel and tumour can be distinguished but contrast levels are different from human liver images. The parenchyma aspect does not show a mean intensity comparable to liver imaging.

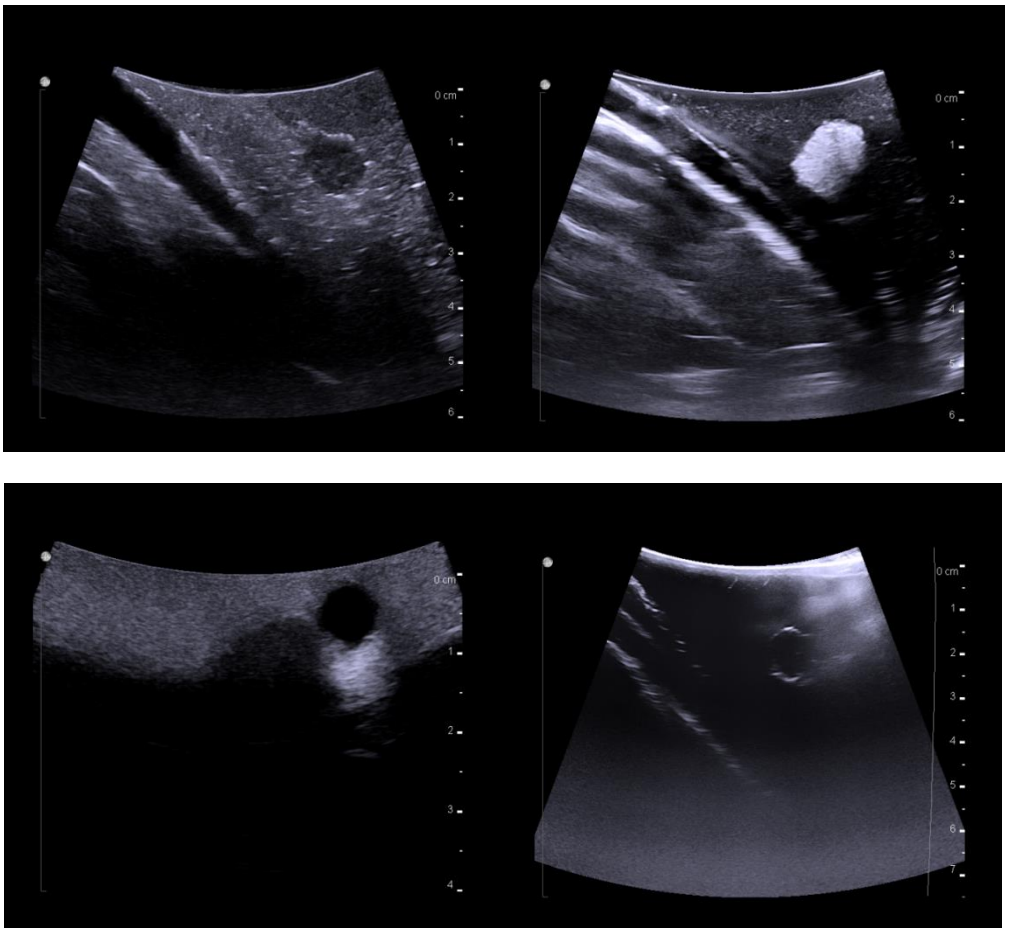

Figure 6: Ultrasound images of the four phantom samples Top left: Candle gel. Top right: Plastisol Bottom left: Silicone. Bottom right: Polyurethane rubber

Table 5: Ultrasound imaging results of four small phantoms.

Material	Diffuse speckle	Contrast parenchyma-vessel/Parenchyma-tumour	Penetration depth
Candle Gel	Yes	Good/Good	>6cm
Plastisol	Yes	Sufficient/Good	5cm
Silicone	Yes	Good/Good	2cm
Polyurethane	No	Bad/Bad	4-5cm

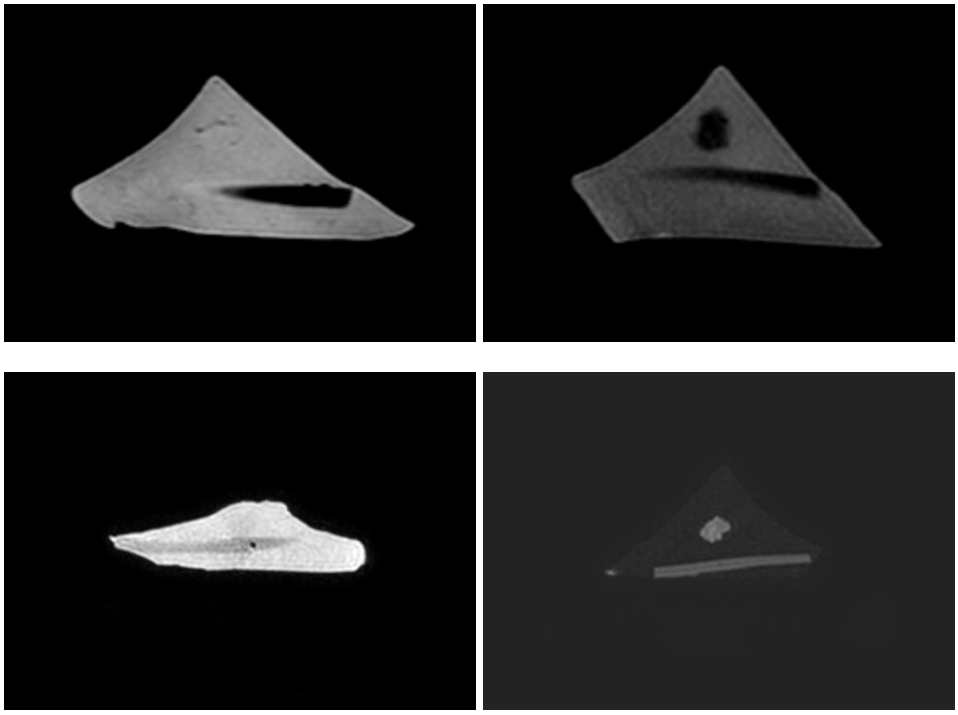

Figure 7: MRI imaging of the four small phantoms. Top left: Candle gel. Top right: Plastisol Bottom left: Silicone. Bottom right: Polyurethane rubber

MRI

On MRI all phantoms show sufficient contrast to segment structures. In patient scans the liver parenchyma shows high signal compared to vessels. In three of the four samples this is the case, only in polyurethane the parenchyma substitute shows low intensity compared to the vessel and tumour. In all materials the tumour can be distinguished. In candle gel the contrast of the tumour with the parenchyma is bad.

Table 6: MRI imaging results of four small phantoms.

Material	Parenchyma signal intensity	Contrast parenchyma-vessel	Contrast parenchyma-tumour
Candle Gel	Good	Good	Bad
Plastisol	Sufficient	Good	Good
Silicone	Good	Sufficient	Bad
Polyurethane	Bad	Good	Good

Structure
All phantoms were presented to surgeons and investigators that work with liver specimens regularly. In terms of realistic feeling polyurethane scores worst. The material is stiff and can hardly be squeezed with the ultrasound probe. The silicone mixture used by Pacioni *et al.* [58] produces a softer but slimy consistency which does not keep its shape. It is deformable however it does not return to its original shape. Various attempts were made to adjust the composition by excluding slacker, thinner and/or vaseline oil but none resulted in a stable result. Plastisol and candle gel are flexible and elastic materials and score the best. Gentle ultrasound probe pressure causes realistic deformation and the material returns to its original shape. Candle gel is more vulnerable for tears than plastisol which can be folded completely, an aspect of human liver tissue that was highlighted by surgeons.

2.1.4 Selection conclusion

The final choice of parenchyma substitute material is candle gel. Based on the results we can conclude that ultrasound performance was very realistic. Silicone and polyurethane rubber are not feasible because of the bad ultrasound performance. In MRI imaging all materials show sufficient or good contrast between parenchyma and vasculature which allows for easy segmentation. Polyuretane has a low signal intensity which would make segmentation of the liver contour difficult. In terms of practicality, the gel is easy to obtain via multiple resellers and the least expensive option. Candle gel melts at 68°C and does not produce toxic fumes, whereas plastisol melts at 180°C and does produce toxic fumes. Also, candle gel is reusable in contrast to silicone and polyurethane that are not. These benefits make candle gel the most suitable materials to use and outweigh the lack of parenchyma-tumour contrast. Because of the This problem is expected to be overcome by using an additive for the candle gel to influence the density [61] or by using a different material as tumour tissue[73].

2.2 Vasculature

2.2.1 Material candidates

The consumer grade bathroom silicone that has been used in the previous chapter is not feasible for a complex shape due to its thick consistency. This silicone has a shore hardness of 28A. Printing of materials with an equal, or lower shore hardness is not easily accessible. Vasculature structures have to be flexible in order to follow the movement of the parenchyma when handling the phantom or applying probe pressure. Stiff vessels will most likely damage the parenchyma in these situations. Furthermore, the vasculature substitute should not cast acoustic shadows that hide the tissue behind the vessel. This is not the case in human liver ultrasound.

Three methods of creating the vessels have been tested; printing the vessels in Gel-lay (Kai Parthy-LayFilaments, Cologne, Germany), printing in Elastic Resin™ (Formlabs, Somerville, USA) and printing in PVA first and then applying Dragon Skin 10 silicone (Smooth On, Inc., Macungie, PA, USA).

Gel-lay
Gel-lay filament is the cheapest material of the three and can be printed with FDM-printers which are widely available. Gel-lay is a combination of TPE-elastomer and PVA. The finished print is rigid but when placed in water, the PVA dissolves and leaves a microporous flexible product. Its shore hardness is not given by the manufacturer but is estimated by experienced users at 40A.[74] This end product could function as the vascular tree in the phantom. No literature was found using this material for ultrasound or medical phantoms.

Elastic Resin

Elastic resin can only be printed with the manufacturer's 3D printer and is more expensive than Gel-lay. The printers and resins of Formlabs are widely used in medical applications such as dentistry and orthopedic surgery. The stereolithography (SLA) printing method has a higher accuracy compared to FDM printing. If not post-cured with UV light, elastic resin prints have a shore hardness of 30A.[75]

Dragon skin

Applying silicone on a PVA product is another method to obtain an silicone vascular tree. In a study describing the development of a newborn life support manikin [76] a PVA printed airway is dipped in Dragon Skin 10 silicone several times to obtain a layer of silicone.[57] This dipping leaves much residue each cycle. A method to avoid this is adding a thickener to the silicone. By doing this the silicone becomes thick enough to brush without altering the final material properties. This Dragon Skin silicone has a shore hardness of 10A.

2.2.2 Selection methods

Selection of vasculature substitute is done by phantom experiments. A simplified portal vessel branch is replicated using the substitute materials. This portal vein was derived from a patient scan and the most peripheral vessels and bifurcations were removed to result in a structure with two levels of bifurcations (Figure 8). The structures were produced and embedded in parenchyma substitute. The vasculature was evaluated by ultrasound and MRI.

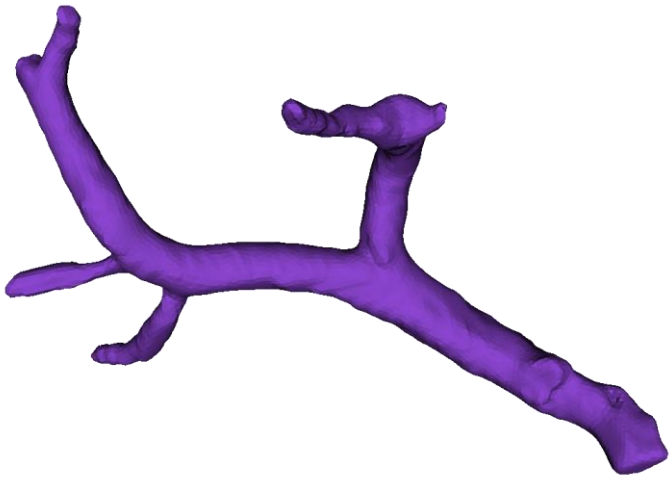

Figure 8: 3D model of a simplified portal vein. The structure was used in phantom tests to find vasculature substitute material.

Gel-lay

The portal vein model was printed in Gel-lay using an Ultimaker 3 (Ultimaker B.V., Geldermalsen, the Netherlands) FDM printer. The advised print temperature of 225-235°C was used.

Elastic resin

Printing in Elastic resin can produce highly detailed flexible models of the vasculature. Vessels can be printed with a minimum wall thickness of 0.4 mm although prints are likely to fail and contain holes. Therefore, the portal vein was printed with a wall thickness of 0.5 mm.

Dragon Skin

A portal vein printed in PVA was brushed with Dragon Skin 10 with added thickener. A layer of approximately 2 mm was applied and set to cure. The next day, the silicone was removed from the print and checked for holes. Remaining holes were sealed again with Dragon Skin 10.

2.2.3 Selection results

Gel-lay

The printing of Gel-lay prints was not successfully completed. As pictured in Figure 9, printing layers of the Gel-lay vasculature separate before the prints could be embedded in a phantom. An attempt to solve this problem was made by altering the printer settings such as extrusion temperature and printer bed temperature but this did not result in a successful print.

Figure 9: Layers of the Gel-lay print that was tested as vasculature substitute have separated after printing and washing.

Elastic resin

Vasculature has been printed in Elastic resin. Figure 10 shows a photograph of the finished prints. During the printing process, the left branch of the portal vein failed twice. Figure 11 pictures the difference of a phantom with the vasculature print still embedded and after extracting the print and filling the remaining cavity with water. After extraction the acoustic shadows are no longer present.

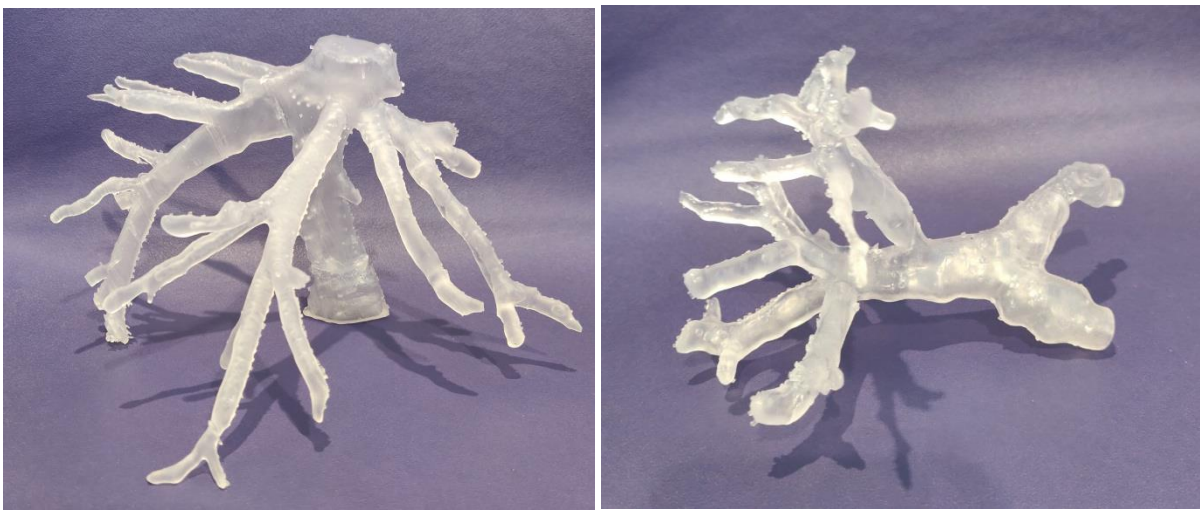

Figure 10: Photographs of the 3D printed hepatic vein(left) and portal vein(right) in Formlabs Elastic resin.

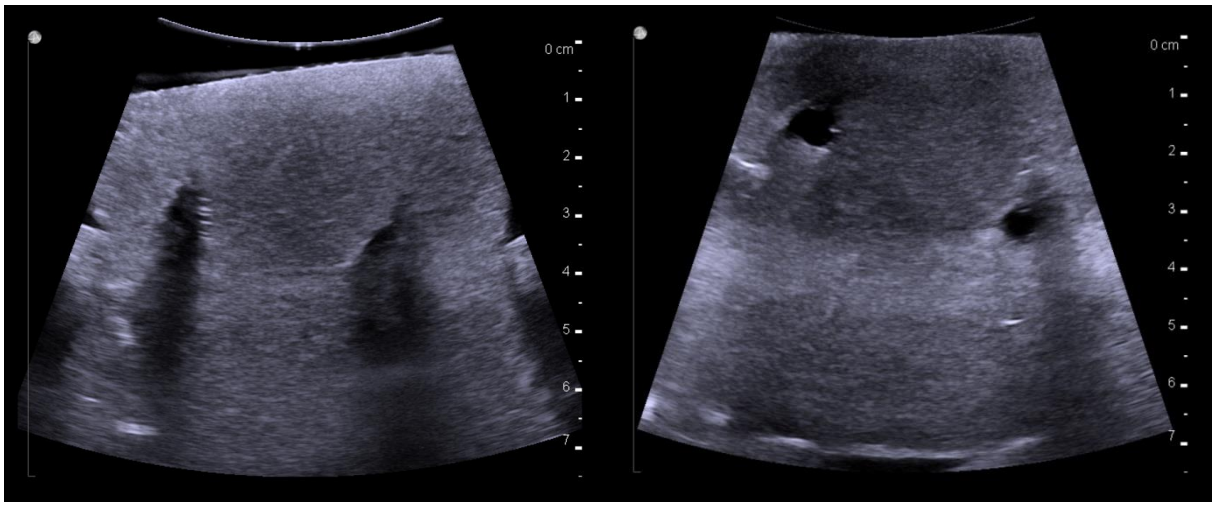

Figure 11: Ultrasound images of a candle gel phantom with vasculature created using Elastic resin. Left: Elastic resin print embedded in phantom. Right: Elastic resin print removed from phantom, the remaining cavity is filled with water.

Dragon skin

The Dragon Skin brushed vessel (Figure 12) was embedded in a cylindrical phantom. It was imaged using ultrasound and MRI. Figure 13 shows ultrasound and MRI imaging of the phantom. In the ultrasound image the vessel is picture together with a tumour. The vessel casts an acoustic shadow that prevents imaging of material behind the vessel.

Figure 12: PVA portal vein print with brushed on Dragon Skin 10 silicone.

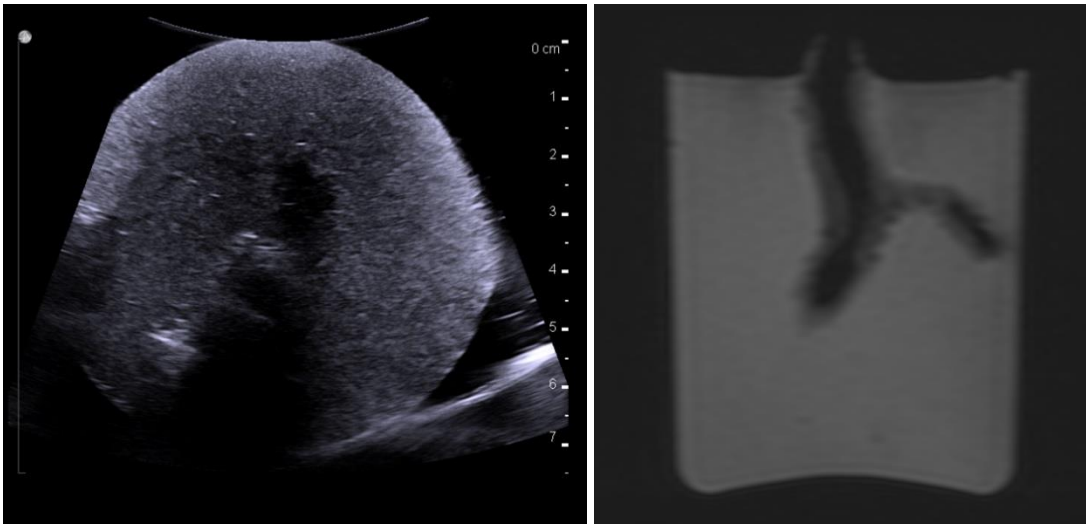

Figure 13: Left: Ultrasound image of Dragon Skin vessel inside candle gel. The hyperechoic tumour can be seen. Underneath is the hypoechoic vessel casting an acoustic shadow. Right: MRI image of the same Dragon Skin vessel.

2.2.4 Selection conclusion

The Gel-lay print could not be tested on imaging performance. Dragon skin and Elastic resin embedded in candle gel produced acoustic shadowing and can therefore not be used as a vasculature substitute. An optimal way of producing realistic looking vasculature was found when a structure printed in Elastic resin was extracted from the candle gel. The cavity that remained filled with water and when imaged using ultrasound, the entire structure including the smallest branches could still be observed. Some damage to the parenchyma was seen but this was not visible on US or MRI. As a result, the selected method to produce vasculature substitute is printing a hollow structure, identical to the segmentation in the preoperative model, in Elastic resin. Then, extracting this print from the phantom once cast, and finally filling the resulting cavity with water. Using this method results in a candle gel phantom with accurate vasculature showing seemingly anechoic aspect.

2.3 Tumours

The tumour material selection was in continuation of the parenchyma selection results. In the parenchyma material selection, the candle gel phantom and the embedded tumour were made from candle gel with added MgO_2 powder. The tumour contained a lower concentration of MgO_2 powder resulting in a hypodense aspect. On MRI, the intensity difference between parenchyma and tumour was minimal as can be seen in Figure 7. The tumour material selection focused on obtaining MRI contrast in addition to the US contrast already present in the small phantom used in paragraph 2.1

2.3.1 Tumour selection methods

Several tumours were embedded in a candle gel phantom to find a way of producing both ultrasound and MRI contrast. Spherical tumours of approximately 1.5cm where produced using a flexible mold. These tumours where embedded in a coffee cup size candle gel phantom and imaged using ultrasound and MRI.

2.3.2 Tumour selection materials

As Vieira *et al.* [77] shows candle gel in combination with carnauba wax is suitable for creating different kinds of abnormalities. In diagnostic imaging of patients, the ultrasound aspect of malignancies differs between lesions. The echo intensity of the lesions can be influenced by the amount of magnesium dioxide added to the material and the MRI contrast is realized by adding carnauba wax to the mixture.[77] To find the optimal tumour composition several lesions containing different concentrations of carnauba wax were made. Besides, gelatin was tested as a tumour substitute material.

2.3.3 Tumour selection results

In Figure 14, US and MRI images of three different tumour compositions are shown. Tumours containing 4 percent carnauba wax (A) show contrast on MRI while tumours containing 2 percent carnauba wax (B) do not. A gelatin tumour (C) shows high contrast to candle gel but appears to be disc shaped.

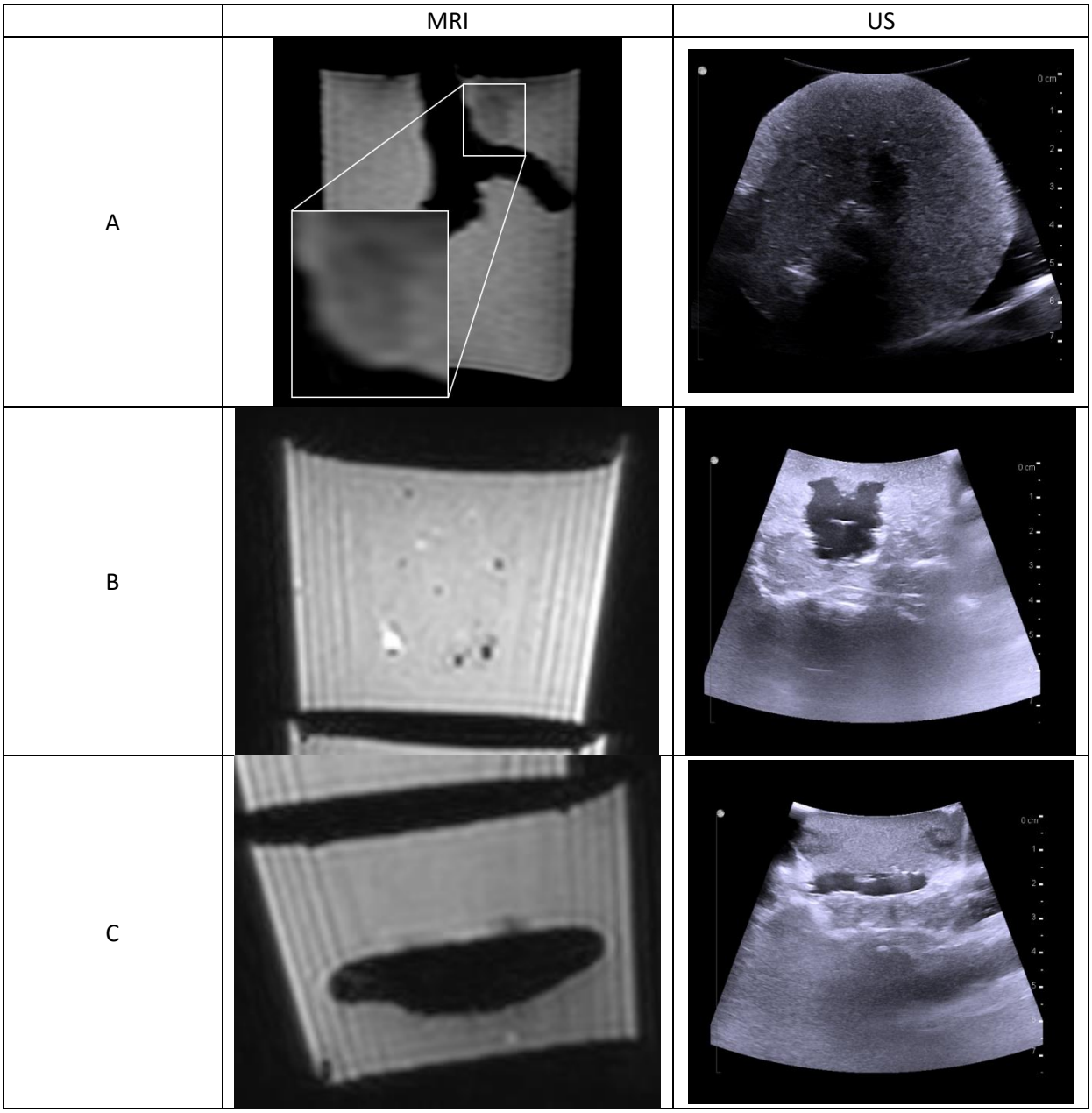

Figure 14: Ultrasound and MRI images of three different tumours, embedded in candle gel. A: A tumour containing 4% w/w carnauba wax. B: A tumour containing 2% w/w carnauba wax can barely be seen on MRI. C: A gelatin tumour embedded in candle gel.

2.3.4 Tumour selection conclusion

Gelatin lesions perform well on both US and MRI. However, the embedded spherical tumour melted after the hot candle gel was poured around it, this resulted in a disk-shaped lesion (Figure 14). Because the geometry of an embedded tumour must be preserved, gelatin is not suitable as tumour substitute material.

Hypodense lesions that produce sufficient MRI intensity contrast to be segmented as well can be realized by adding a small amount of MgO_2 powder and carnauba wax to the candle gel. The concentration of MgO_2 powder should be lower than the surrounding parenchyma to produce hypodensity, the concentration of carnauba wax should be 3%. A concentration of carnauba wax higher than 4% will result in acoustic shadowing on ultrasound. On the other hand, a tumour model

with a concentration of carnauba wax of 2% does not show MRI contrast sufficient for segmenting the lesion.

2.4 Conclusion

From the material selections described in this chapter, a final selection of tissue substitutes can be derived. First, to mimic parenchyma, candle gel mixed with 1 g MgO_2 powder per 100mL of candle gel is used to produce realistic ultrasound speckle on ultrasound and a high intensity on MRI. The candle gel is vulnerable for air bubbles but this can be prevented by placing the molten gel in a vacuum chamber before casting. Vasculature materials have been tested but a material with the desired ultrasound properties has not been found. Instead, a cavity in the phantom filled with water shows realistic aspect of real liver vasculature. The geometry of the liver vasculature can be produced by 3D printing the vasculature outline in Elastic resin. This print is embedded in the phantom and extracted when the candle gel has set. The elastic properties of Elastic resin allow for extracting the entire vascular tree at once without causing major damage to the parenchyma substitute. Tumour models are produced by using spherical molds. The tumour material is candle gel with 3% w/w carnauba wax to realize MRI contrast and 1 g of MgO_2 powder per 500 mL of candle gel to produce hypoechogenic aspect compared to the parenchyma.

3. Phantom study

3.1 Introduction

The material selection and method study described in Chapter 2 results in a method to create a multimodal liver phantom. In this chapter we describe the productions of a liver phantom based on a clinical patient scan. A preoperative model from this scan functions as the design of the phantom. Geometry of the parenchyma and vasculature is identical to the scan. Malignancies in the phantom are different than in the preoperative model to present useful cases. A CT and MRI scan of the phantom are made to evaluate the imaging performance and geometry. Ultrasound aspect is evaluated and compared to ultrasound aspect in patients. Finally, practical use of the phantom is evaluated in an experimental setup identical to an intraoperative setup.

The patient-specific phantom is based on the 3D model. To create a similar geometry 3D printing techniques and casting techniques are used. In the following sections the methods of shaping the materials and realizing a patient-specific phantom are presented.

3.2 Method

3.2.1 Parenchyma

To realize a patient-specific liver phantom the parenchyma substitute needs to be shaped as the segmented liver outline. To do this a cast is needed, 3D printing offers a fast and affordable way to construct a custom mold.

Candle gel was used as parenchyma substitute. The gel has a melting point of ca. 68°C. 3.2 liters of gel were used for the phantom. The gel was heated until completely melted. 20 teaspoons of magnesium-dioxide powder were added under continuous mechanical stirring. Brown dye was added to approach realistic human liver color.

The STL files created from the patient scan were imported in open-source software Blender (Blender Foundation, Amsterdam, The Netherlands) for the creation of a casting mold. The basic concept of the casting mold is a shell in the shape of the liver contour that is divided in three parts to extract the phantom once cast. A negative of the liver outline is created by performing a Boolean difference operation with the parenchyma segmentation on a cube. The cube is divided in a top half and a bottom half. The bottom half is once more divided in a left and right half (Figure 15). To finish the mold, pins and holes are created on opposing parts to obtain a constructible mold. Excess material is removed from the design to save printing time and costs. Additionally, two holes are created in the top parts that are used to pour in the candle gel. Risers are added to these pouring holes that prevent empty spaces that would otherwise appear because the candle gel shrinks when it cools down. To position the tumours, small holes are created in the top part of the mold, above the tumour location. The tumours are fixated on a wire that is put through these holes, just before the candle gel is poured.

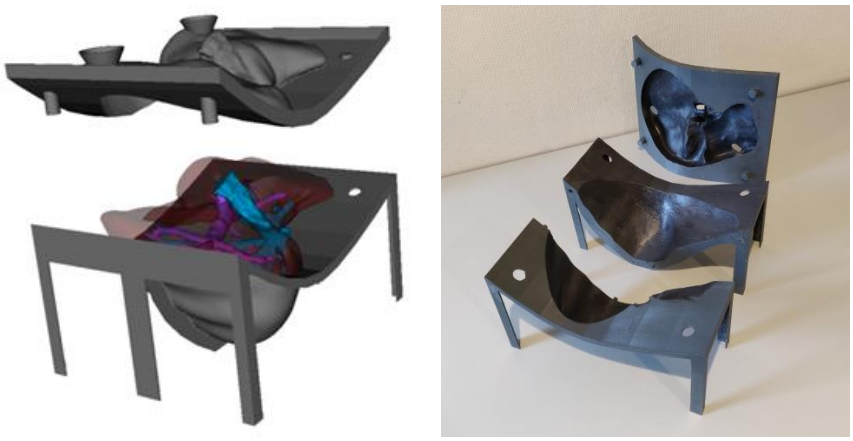

Figure 15: 3D model of the casting mold. The model consists of three parts that can be constructed to form a casting mold in the shape of the parenchyma. Left: 3D model of the casting mold and the 3D model pictured inside. Right: A photo of the physical 3D printed mold.

3.2.2 Vasculature

The STL files of the hepatic vein and portal vein were used to create a 3D printing model. Meshmixer software (Autodesk Inc., San Rafael, USA) was used to create a hollow model with a wall thickness of 1.5mm. This prevents failure of the printer due to thin walls collapsing, on the other hand the wall is thin enough to be flexible. The structures were printed in Elastic Resin™ using a Formlabs Form 2 printer (Formlabs, Somerville, USA). To prevent remaining resin inside the hollow structures 2mm holes are created at the end of each major branch. Once the printer had finished, the prints were washed with isopropyl alcohol and post cured for 2 minutes with UV-light. The holes at the end of the main branches are closed with consumer grade silicone sealant. Finally, the structure is placed in the mold as pictured in Figure 16 (top).

3.2.3 Tumours

The tumour location and size are adapted to be useful to both ablation and excision cases, therefore they are different from the clinical scan. Two central lesions and two peripheral lesions are inserted to have a phantom useful for simulating different settings. The material to create the lesions is the same candle gel as is used for the parenchyma, with the addition of carnauba wax.

3.2.4 Assembly

The liquid candle gel was then placed in a vacuum chamber at -80kPa for approximately 5 minutes. Subsequently, remaining foam on top of the gel was removed. The inside of the liver mold and the vasculature was coated with Universal Mold Release (FormX, Amsterdam, The Netherlands). The vasculature prints were fixated in the mold. The tumours were fixed on wire run through the corresponding holes in the top part of the mold. The mold was assembled and sealed with consumer grade silicone sealant. The gel was then poured into the mold and set away to cool.

3.3 Results

After 24 hours the phantom was removed from the mold and the printed vasculature was extracted carefully. The hepatic vein structure is removed in one piece, the portal vein structure is cut at the first portal bifurcation and left and right branch are removed separately. After removal the remaining cavity

is completely filled with water and the outside was coated with Mouldlife Super Baldiez (Mouldlife Ltd., Sufflok, United Kingdom) to protect the material from damage.

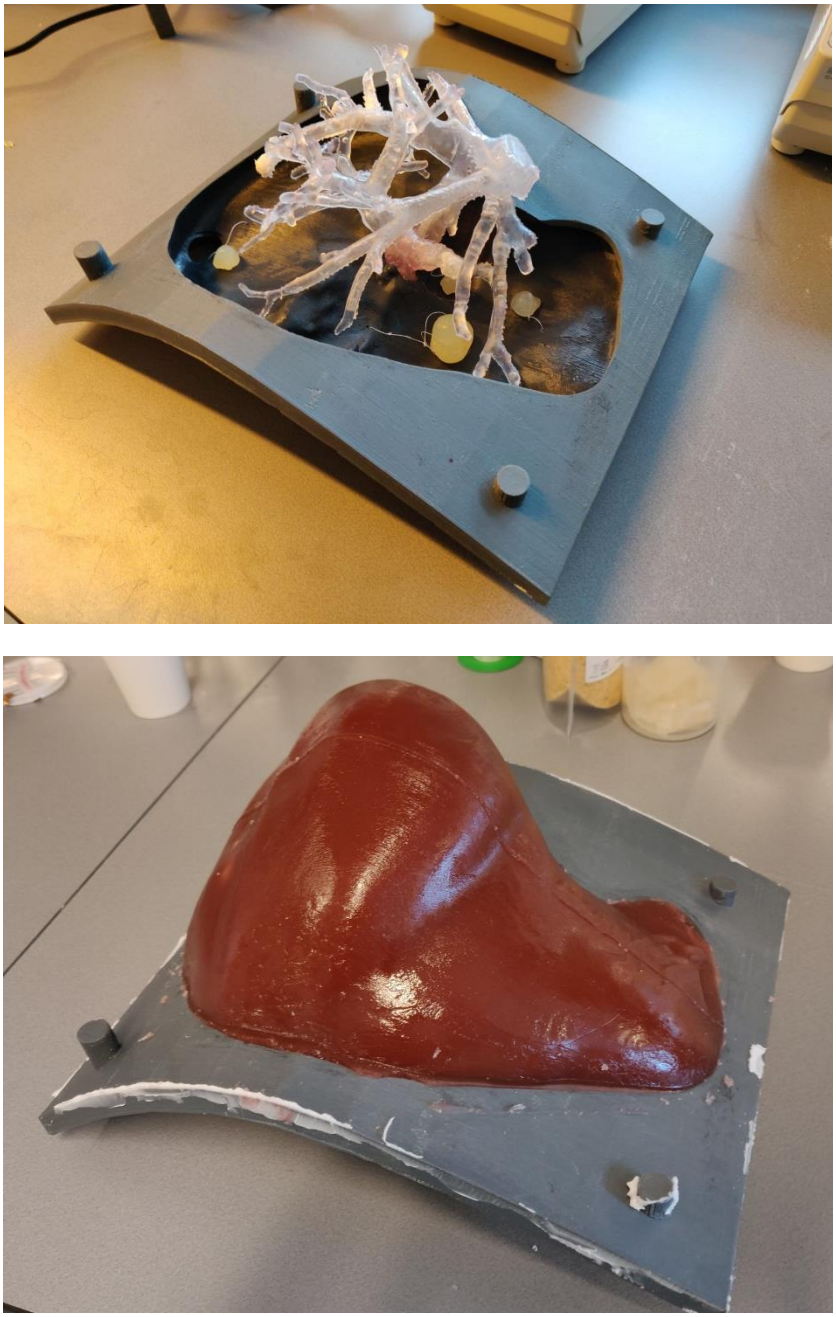

Figure 16: Top: Top part of the mold with attached vasculature and tumours.
Bottom: Top part of the mold after casting the parenchyma substitute and opening the mold.

3.3.1 Ultrasound

Ultrasound images were acquired and contrast between lesions and parenchyma was assessed by inspecting the intensity along a line through the vessel. The profile is compared to intraoperatively acquired US images of a human liver. The shape of the intensity profile describes the ultrasound aspect of the vessel in the sample. The difference in mean pixel value quantifies the contrast on the ultrasound image. The results are presented in Figure 17 where a mean pixel value of approximately 100 can be seen before and after the vessel, both plots drop to an intensity of 0 for the lumen.

During ultrasound imaging of the phantom, the lesions are not visible. By following the tumour positioning holes in the liver mold the location of the tumours was approached. In none of the four tumour locations a structure could be distinguished.

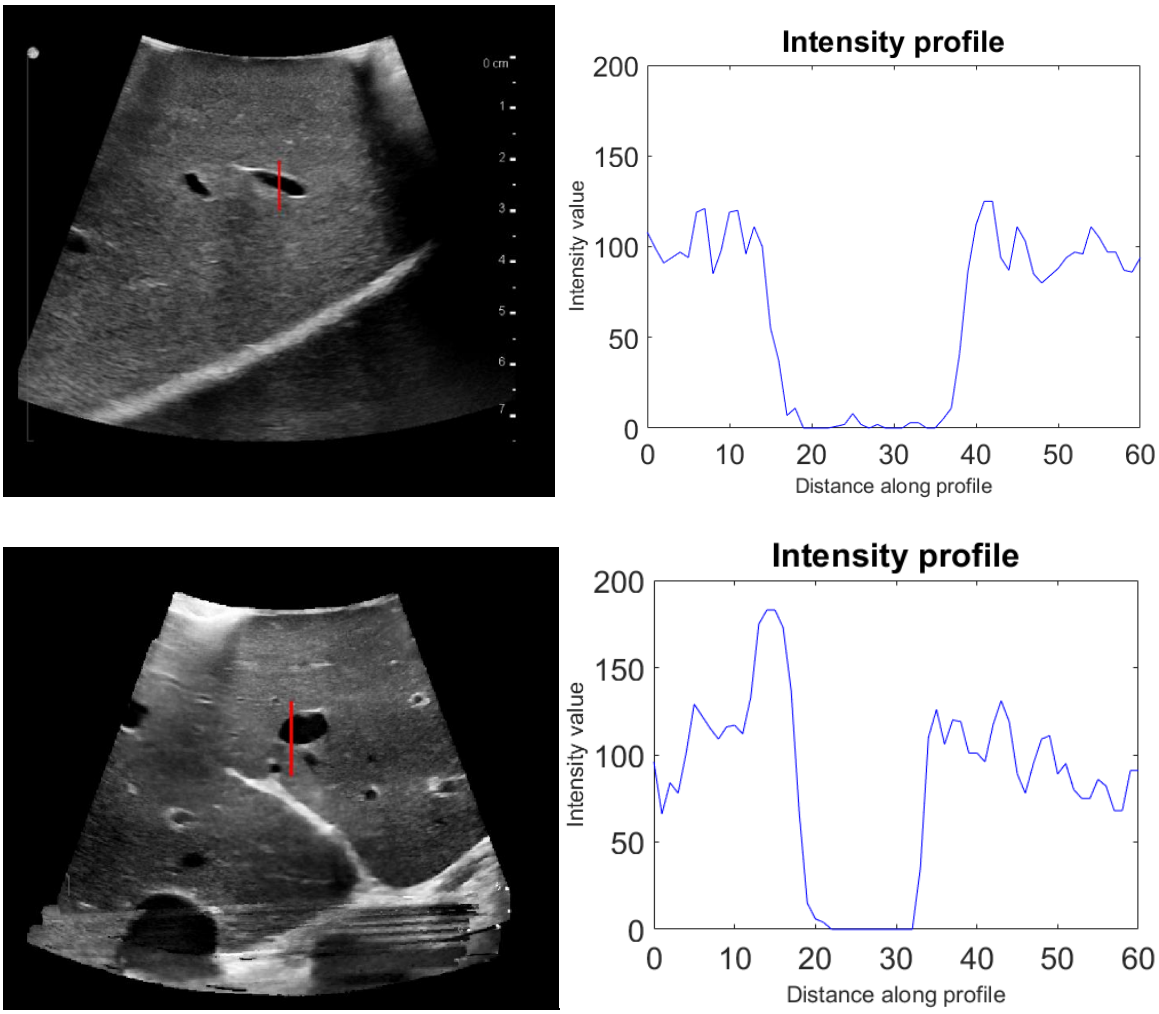

Figure 17: Top: Ultrasound slice of the phantom. The intensity profile across the red line is shown in the plot. Bottom: Intraoperative ultrasound slice of a patient. The intensity profile across the red line is shown in the plot

3.3.2 **MRI**

3D FFE-mDixon multiphase MRI-scans were acquired using Gd-EOB-DTPA-enhanced (Primovist® In Europe, Eovist® in the USA, Bayer Healthcare, Germany) for diagnostic liver imaging, as source for segmentation of the 3D model.[78] The scan is made using a Philips Achieva, 1.5T scanner (Philips Healthcare, Best, The Netherlands), with a slice thickness of 2mm. The hepatobiliary phase scan shows high contrast between parenchyma, vessels, bile ducts and pathologies due to the high concentration of the contrast agent gadolinium in the parenchyma and bile ducts.

On MRI the vasculature cavities are visible. The level of contrast is sufficient to segment the vasculature and create a 3D model shown in Figure 18. To compare the level of contrast between the phantom scan and the clinical scan an intensity profile is created. A line is drawn across a vessel and the contrast difference between parenchyma and vasculature is visualized. The phantom shows a comparable but slightly higher contrast of approximately 150 for the parenchyma and 0 for the vasculature.

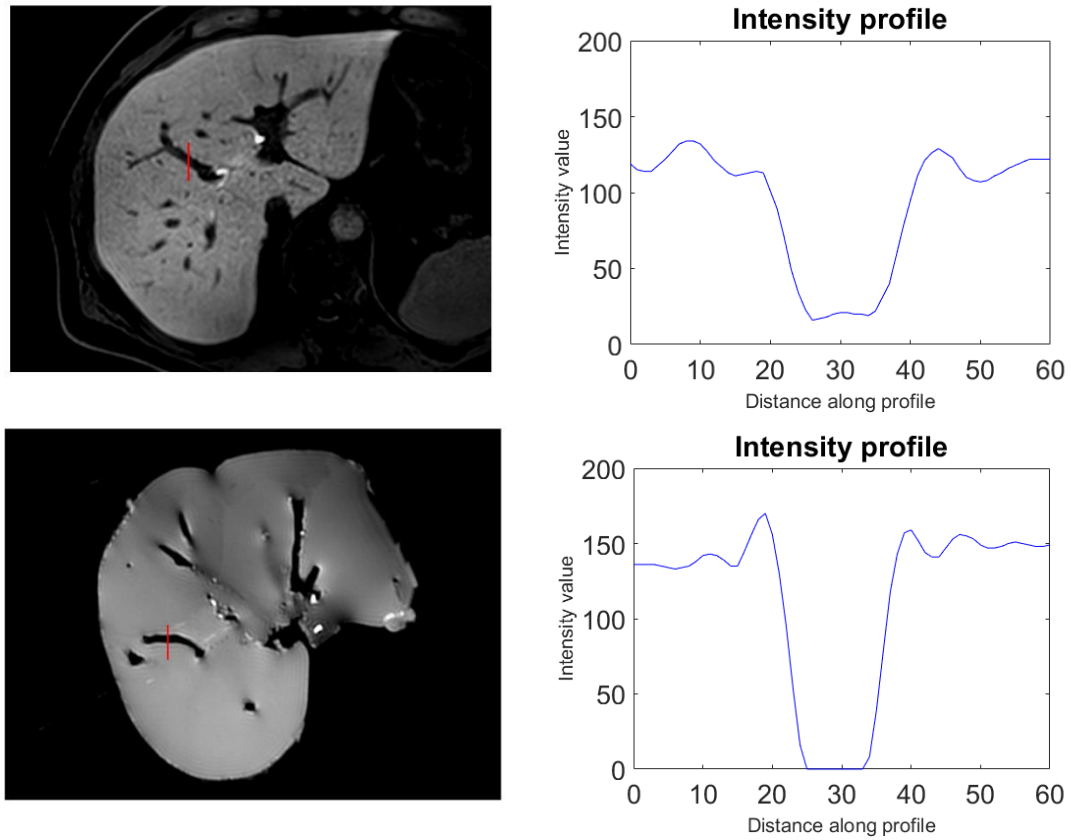

Figure 18: Top: MRI slice of the patient. The intensity profile across the red line is shown in the plot. Bottom: MRI image of a phantom. The intensity profile across the red line is shown in the plot

On MRI, the embedded tumours can also not be found. The locations where the lesions should have been present were approached by examining the preoperative model, but no lesions could be distinguished. The entire phantom was examined for traces of deformed or delocalized lesions but the parenchyma substitute was isointense throughout the entire scan.

3.3.3 **Geometry**

The images are exported in DICOM format and imported into 3D Slicer software (http://slicer.org).[79] The liver contour was automatically extracted using a custom module of 3D Slicer.[80] Subsequently, the hepatic vein, portal vein are segmented using a 3D threshold brush, based on intensity levels. Similarity between the phantom and model has been assessed by means of Hausdorff distance. Segmentations of the hepatic vein, portal vein and liver outline on an MRI scan of the phantom are compared to the preoperative model that the phantom is based on. The metrics that are used have been used for the evaluation of segmentation algorithms.[46, 47]

A segmentation of the liver phantom is shown in Figure 19. The phantom structures were segmented using the same method as the preoperative scans, using 3D Slicer.

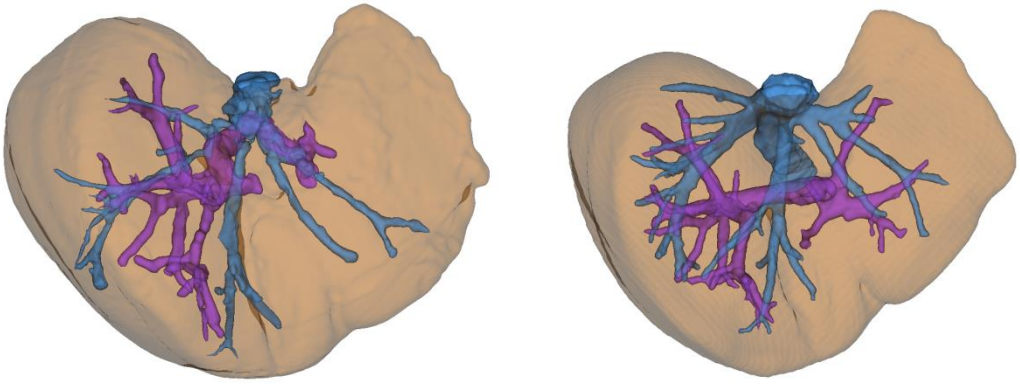

Figure 19: Left: The 3D model based on an MRI scan of the phantom. Right: The 3D model of the preoperative scan that the phantom was based on

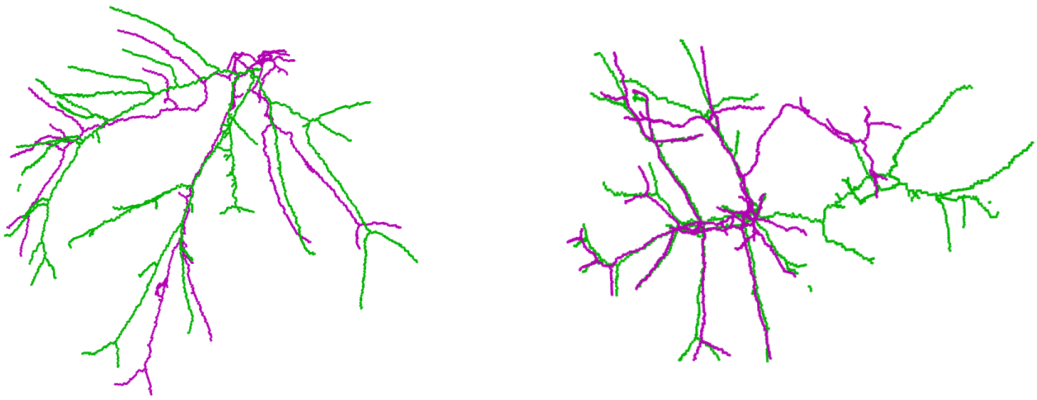

Figure 20: Centerlines of preoperative model (green) and phantom (purple) segmentations show similar branches and bifurcations in hepatic vein (left) and portal vein (right) structure

Volume was calculated of the clinical liver segmentation and of the phantom liver segmentation. The clinical segmentation had a volume of 3088.78 cm^3. The phantom segmentation had a volume of 3022.54 cm^3, 66.24 cm^3 (2.14%) less volume than the patient scan.

The liver segmentations of the liver outline are registered using iterative closet point (ICP) method.[83] In Figure 21 the patient liver outline is shown in green and the phantom outline is shown in red. The registration results in an overlay with a dice coefficient score of 0.94. The average Hausdorff distance of the registered models is 2.3 mm (5.7 mm 95%) with a maximum of 21.8 mm at the edges of the phantom. The Hausdorff distance can be interpreted as the greatest of all the distances from a point in one set to the closest point in the other set.

The vascular anatomy present in the phantom shows a high resemblance to the preoperative model of the patient scan. In Figure 20 the centerlines of both segmentations are presented after manual fiducial registration using five points. The portal structure on the right clearly shows the missing left branch that was lost during printing the vasculature structure used in the phantom.

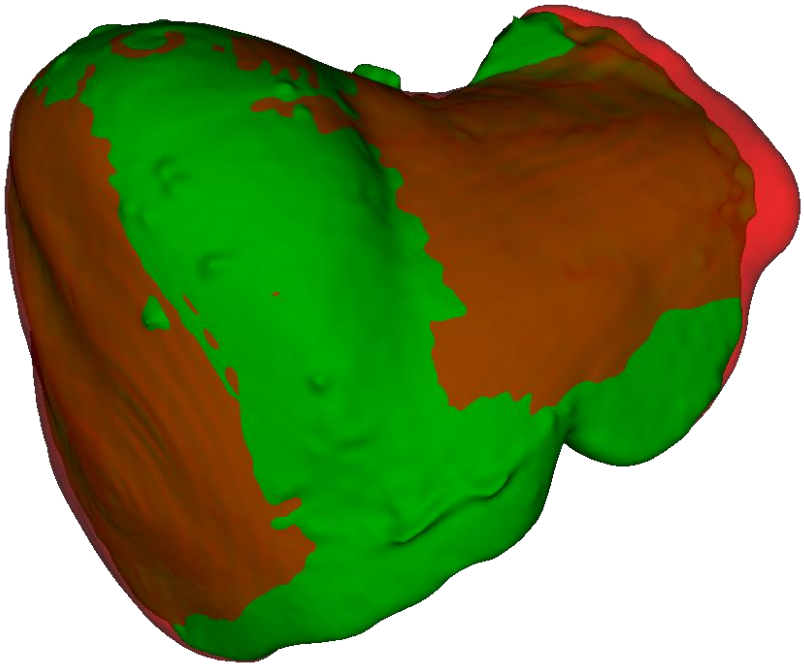

Figure 21: Segmentations of the clinical liver outline and phantom liver outline registered using iterative closest point. In green the liver outline of the patient scan, in red the segmentation of the liver outline of the phantom.

3.3.4 **Practical use**

Navigation simulation

The created phantom has been used in a navigation setup identical to the one used in the operating room. The 3D model derived from the MRI scan of the patient functioned as preoperative scan. Landmark registration was performed using points on the liver contour. After registration using these landmarks the preoperative model was registered to the "operating scene". Initial registration of the model to the operating scan was successful. Probe orientation as imaged in the software corresponded to the probe orientation in the setup. As pictured in Figure 22 correspondence between the hepatic vein (blue) and underlying hyperechoic cavity wall can be seen. However, the portal structure (purple) has a mismatch as no corresponding structure can be seen on the ultrasound slice beneath.

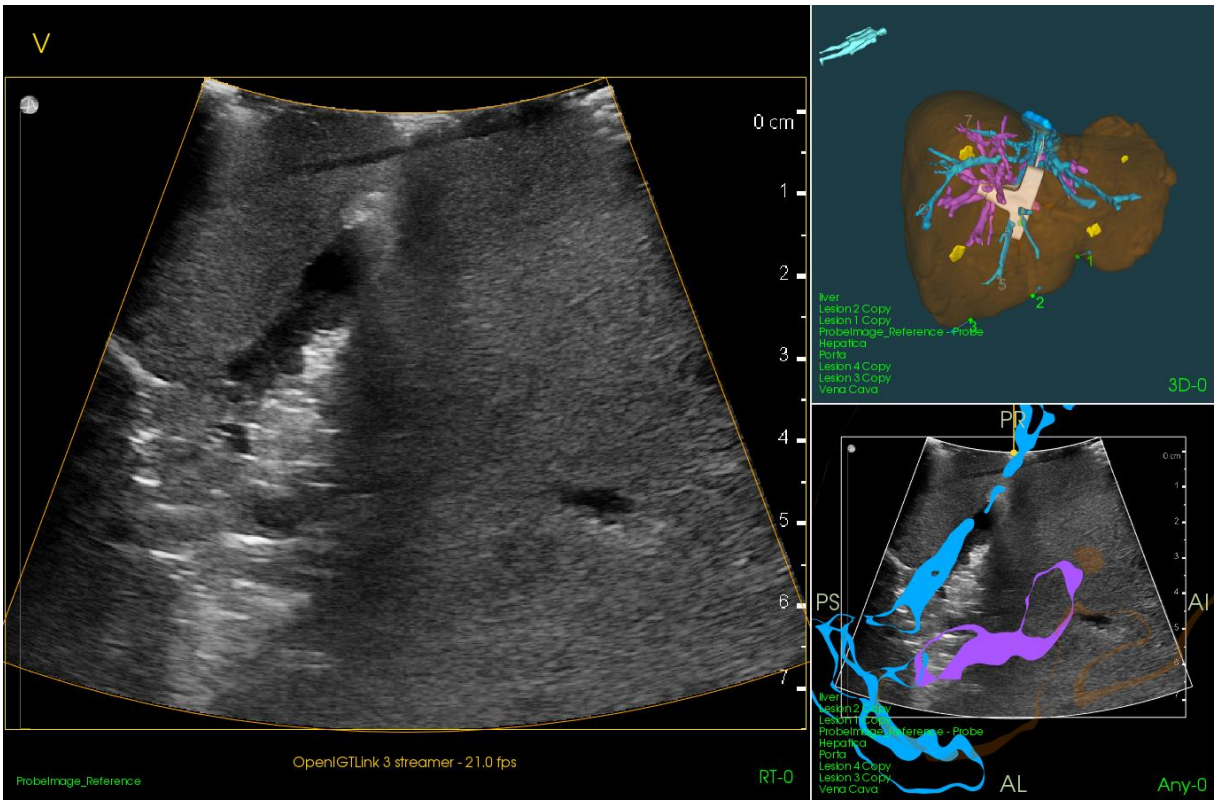

Figure 22: Screenshot of the US-MRI navigation software. Left: Ultrasound image as recorded. Top right: Preoperative model of the phantom including the ultrasound probe position. Bottom right: Overlay of the model structures on the ultrasound slice.

Ablation experiment

A simulation setting was created to provide two surgeons with an opportunity to practice working with a new US guided ablation device (See Figure 23). A single ultrasound probe producing two image planes was used to image the vascularity. The probe is equipped with a guide for ablation needles. Three trajectories are possible that guide the needle at an exact angle into the imaged plane. Corresponding lines on the ultrasound image show the trajectory that the needle will follow when inserted through one of the options. This method was attempted once during surgery but demands practice and therefore was not used after. This application shows that the phantom can be used to simulate a patient in development of the US-MRI navigation method (Figure 24). Organ manipulation, probe manipulation, ultrasound imaging and needle insertion were all scored high by three experienced liver surgeons when presented the questionnaire in Table 7. The phantom presented here does offer the opportunity to practice in a realistic simulation and brings clinical implementation closer.

Figure 23: A needle is inserted using ultrasound guided techniques on a smaller phantom containing vasculature.

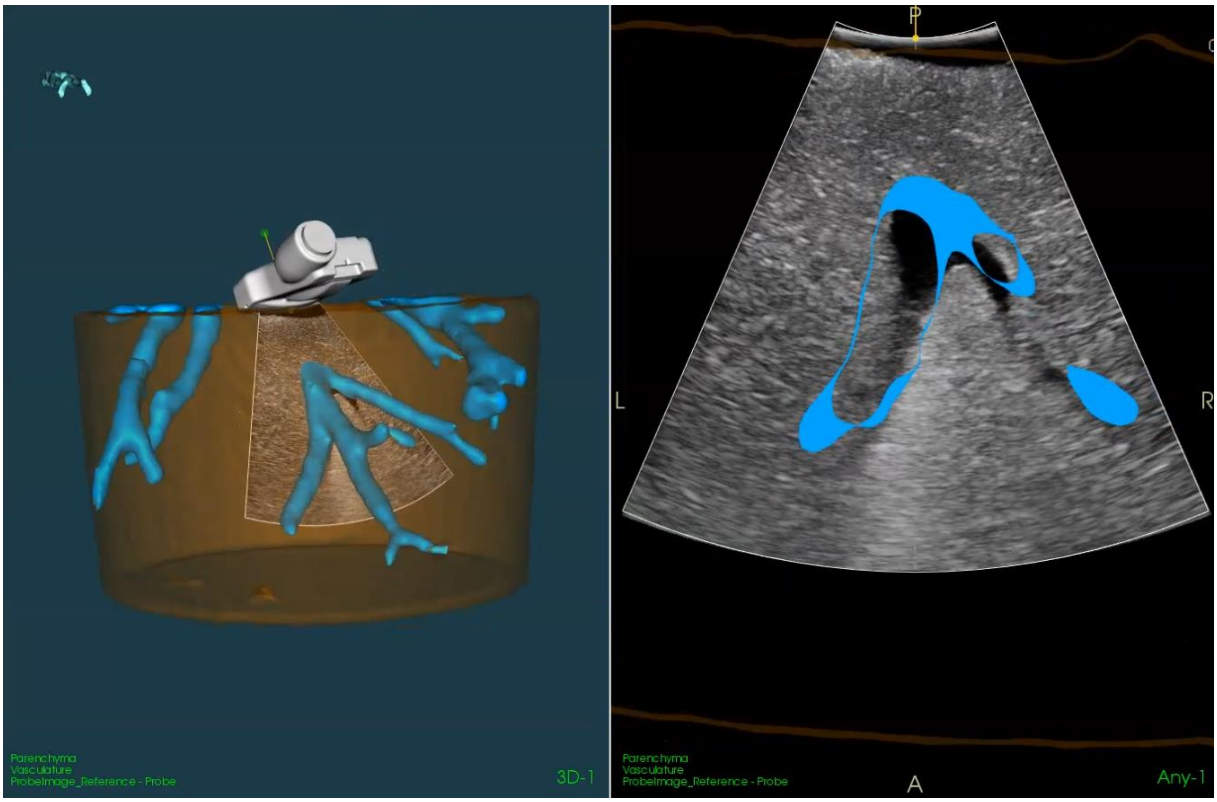

Figure 24: Screenshot of a registration performed using surgical navigation software on the phantom used during the ablation experiment.

Deep learning vessel segmentation

Images obtained from the phantom were used as an input for a deep learning method to automatically segment vessels from ultrasound images. This segmentation method is still under development and will be implemented in the workflow of surgical navigation as a part of automatic US to MRI registration. The network was able to segment the vessels in the phantom with a result comparable to segmentations from patient data US images. The phantom can therefore be used to test the implementation of the automatic registration when the deep learning segmentation method is finished. Registration on the phantom can be performed multiple times by developers to find the best approach or by surgeons to get used to the process.

Table 7: Questionnaire on practical use of the liver phantom. The score ranges from 1 (Strongly Disagree) to 5 (Strongly Agree)

Statement	Surgeon 1	Surgeon 2	Surgeon 3
From the outside the phantom looks realistic	5	4	5
Probe manipulation feels realistic	4	4	3
Organ manipulation feels realistic	4	4	3
Ultrasound aspect of the parenchyma looks realistic	4	5	4
Ultrasound aspect of the vessels looks realistic	3	3	5
Ultrasound aspect of the tumours looks realistic	1	1	2
The phantom is pleasant to work with	4	4	4
This setup is a good simulation.	4	4	4
This phantom can be used to develop surgical navigation techniques	4	5	4
This phantom can be used to practice surgery	2	4	4
The needle insertion feedback is realistic	5	4	3

4. Discussion

The goal of this study has been to develop a patient-specific, multimodal liver phantom to support the development of surgical navigation systems and provide a realistic simulation scene for applying new ultrasound guided techniques. Through a series of materials and method tests a final production method has been derived and used to create a phantom. The multimodality has been assessed using ultrasound and MRI. The phantom produces realistic ultrasound imaging of parenchyma and vascularity, similar to intraoperative US imaging in patients. The tumours could not be identified in the final phantom by US or MRI. Vascularity on MRI shows clear contrast which allows for accurate segmentation. The segmentation and production of a 3D model is possible by using the same method as in a patient scan.

4.1 The materials

Two aspects are taken into account to judge the performance of the materials that are used to produce the multimodal phantom, being imaging performance and practicality. First, the imaging performance of candle gel is a strong point of the phantom. The ultrasound imaging is in accordance with the literature and parenchyma and vasculature are assessed as nearly identical to intraoperative imaging by three surgical residents. Besides, commercial phantoms or other scientific liver phantoms do not produce US images with a penetration depth of more than 7cm or realistic vasculature images with multiple bifurcations. An aspect that is not evaluated but must not be forgotten is the difference in speed of sound between candle gel and soft tissue. This difference results in a mismatch between ultrasound measurements and physical geometry of the phantom. Because the phantom was not evaluated on geometry on the ultrasound images this was not identified as a problem during the tests. Also, in the ablation experiment where surgeons approached a defined target with an ablation needle under ultrasound guidance, there was no noticeable image distortion due to the different speed of sound. Hence, the candle gel is appropriate for simulating US-guided ablation procedures.

Vasculature realization by means of embedding 3D printed structures and subsequently extraction of the prints is a newly developed method of accurately reproducing vasculature. The final result is accurate on imaging modalities and the prints are reusable after extraction. All the vasculature that was embedded could be segmented accurately by the same method as used in preoperative models of clinical scans. The vascular tree segmented from the MRI scan showed high resemblance with the patient model and all vessels could be recognized during US examination.

In the future, more material tests can be realized to optimize the phantom. Although vasculature extraction resulted in the desired imaging results, a solid material that shows the same properties can add benefits. The hollow vasculature means the phantom must either be used in a water bath or vasculature must be sealed once the water is inside. The latter has been attempted by melting a plate of clear candle gel to the back, covering the openings that are leading to the vasculature cavities. This method was proven to be difficult as seams leak and because the plate was vulnerable for tears, comparable to the parenchyma. Furthermore, a compatible solid vasculature substitute would eliminate the need for print extraction and filling cavities with water.

A problem that was encountered during practical tests of the phantom was a visible needle trajectory after needle insertion. Contrary to the findings of Vieira *et al.* [50] who reported up to 40 punctures before air tracks became visible in the candle gel, a needle trajectory was visible after just one puncture. No needle trajectories are visible in human liver tissue during or after positioning of ablation

needles and the existence will probably affect the work of the user. Presence of a handful needle trajectories is acceptable however an unharmed phantom is desired at the start of any new experiment involving new punctures.

4.2 The phantom

In the full size liver phantom, desired tumour creation was not successful. The tumour material that has successfully been tested in small phantom experiments was implemented in the liver phantom following the same method. When the phantom was scanned using MRI and examined using ultrasound the lesions could not be distinguished. An additional CT scan was made in an attempt to localize the embedded lesions and complete the 3D model but no lesions were visible either. A deficient carnauba wax concentration in the lesions could be one an explanation for MRI but on ultrasound also a lesion with low wax concentration should be visible. Another explanation is that the tumours dissolved in the surrounding parenchyma. Due to the large amount of parenchyma it takes an excessive amount of time for the liver phantom to completely cool down. It can be imagined that the lesions have re-melted during this cooldown period and have (partially) mixed with the surrounding parenchyma. Due to the much larger ratio of parenchyma to tumour volume the small amount of carnauba wax will then spread out in an undetectable concentration. In order to prevent this several solutions can be imagined. For instance, insertion of tumours after casting and cooling of the parenchyma substitute would prevent re-melting of the tumours. Superficial tumours were successfully implanted but for deeper tumours the cut in the parenchyma that is needed is visible under US as well as unwanted air that cannot be prevented. Another solution is using a different material that does not melt could be an option. Small pieces of polyurethane rubber and silicone were embedded in a small phantom but were not suitable because they reflected or absorbed the US and created acoustic shadowing. A third option that can be thought of is to prevent dissolving of the existing lesions by a protective layer. In Schwaiger *et al.* [66] cling film was used to separate agar tumours from candle gel parenchyma by wrapping them in cling film. From the images in the article it cannot be seen whether the cling film reflects the sound or allows for imaging of structures behind the tumours. If not, a similar approach using a material like cling film could still be a possible solution.

Collapsing vessels is a problem that needs to be addressed. Although the vasculature looks very realistic in the first few days after extracting the prints, small branches in the phantom tend to collapse. Filling the vessels with water and sealing the phantom could be the solution. Sealing the entrance holes of the hepatic and portal vein was attempted by adhesion of pure candle gel. Although this seal was watertight the applied part separated when the phantom was transported and used in practical tests. In the smaller, cylindrical phantom described in paragraph 3.3.4 this was much less of an issue must likely due to the smaller size of the phantom and the positioning of the branches. The smaller size means there is less weight of candle gel to deform the inner cavities and the orientation of the vasculature being downwards during storage means that most of the vasculature is less affected by gravity.

Haptic feedback and needle insertion are scored realistic by two surgeons in a questionnaire. The candle gel shows flexibility approaching that of a human liver. Shortcomings of the material are vulnerability to tearing and the brittle edges when handling. This fragility is the main problem of this phantom. After practical use of the phantom and transporting the phantom from the mold to the operating table and back, major tearing occurred and reparation was needed. The location of the tears was mainly in the area where the vena cava would normally be. The ventral side of the liver where most of the probe manipulation was done, did not suffer notable damage. Reparation of these tears was

possible by heating the inside of the tear until gel started to melt. Subsequently closing the tear results in adhesion and reparation of the tear. Minor damages and tears to the phantom can be repaired in a similar way.

The liver outline of the phantom approaches the outline on the preoperative scan. The patient-specificity has been assessed by comparing the 3D model of the phantom to the 3D model of the preoperative patient scan that the phantom was based on. From the minor difference in volume (2.1%) and the 95-percentile Hausdorff distance of 5.7 mm and a maximum of 21.8 mm it can be concluded that the phantom is an accurate replication of the liver as seen on the patient scan in terms of geometry. The vascular trees of the hepatic vein and portal vein have corresponding bifurcations and trunks of comparable size. The left branch of the portal vein misses a major part of the branch. This is due to failure of the 3D printer. The dimensions of the portal vein print approach the maximum print volume of the printer which probably explains the printer failed twice in printing the final layers. The cause of this failure is expected to be the motion caused by the print bed wiper. Between each printing layer the printer bed moves so the print separates from the printer window. This causes the print to move. When the printer starts printing the next layer the print should have returned to the printing position, although 100 microns above the window, allowing a new layer to be cured underneath. Because the material is flexible the risk exists that the print has not fully returned to the print position when the printer start printing the next layer. This risk increases when the dimensions of the printed part increase. Because the Elastic Resin is a new material, only released in January 2019, this is a problem that might be solved by the manufacturer in the future. In an attempt to prevent this problem, manual support structures were added to the printer task in addition to the automatically generated ones. Cones were placed alongside the vasculature print that would theoretically minimize the possible movement during the printing process. However, the print failed again. For now, reducing the size of the prints seems to be the best option. This would mean either printing the structures in connectable parts or reducing the phantom size in total.

During extraction of the vasculature from the phantom the portal structure separated and two branches were extracted separately. This did not have consequences for the phantom but the structure cannot be used again. In the future, when reusable vasculature is desired, separate printing of the left and right portal branches will most likely be required. The angle usually seen in the portal bifurcation makes it impossible to extract the entire portal structure in one piece without tearing the vasculature print or the parenchyma substitute. When modelling the vasculature print files it is possible to split the file on the bifurcation between the left and right branch of the portal vein. Intuitive design in the 3D modelling process can produce two separate prints that are connectable so that these parts can be embedded together and extracted separately.

In terms of practicality the candle gel has the benefit of being relatively cheap and reusable. Minor damage to the phantom such as surface tears or holes can easily be repaired by using a handheld torch and melting the gel locally. Despite this, major tearing of the final phantom could not be prevented during transport and handling of the phantom during evaluation. The size and weight of the phantom introduced problems that were not found in sample tests. Holding the phantom with bare hands resulted in surface stress that caused tears. The best way to store the phantom was in the 3D printed mold that was used during production. Another method of storage that could be considered is a water bath. The phantom produced in this thesis was stored in a water bath for several days between experiments. Increase of the damage caused with transport and dissection between the left and right liver lobe occurred in the phantom caused by drifting apart on the water surface.

Apart from the difficulties and problems that arise when increasing the scale of a candle gel phantom, it has also been proven usable for other tissues such as small breast phantoms for a study involving augmented reality.

4.3 Requirements validation

In Chapter 1.4.1 a list of requirements for the final product was formulated. Below, an overview is given that states the requirements, if are achieved in the final product or not, including a short statement.

The product should have realistic US, CT and MRI image properties	✓	The US intensity contrast of parenchyma and vasculature is comparable to patient images and the imaging is evaluated as very realistic by three liver surgeons. The MRI intensity is sufficient to be able to segment the vascularity by the same method used in patient scans.
The product can be used with conventional imaging devices.	✓	All images of the phantom were made using standard clinical equipment and configurations.
The product can be used for surgical actions such as incisions, needle insertions and ablation	✓	Incisions and needle insertions are possible. Ablation of the tissue by heat or radio frequent ablation is not possible.
The mechanical properties of the phantom must be close to real tissue, to simulate haptic feedback	✓	Probe tissue interaction was scored realistic by three surgeons in the practical use. The phantom is deformable and returns to its original shape during experiments.
The product should not be toxic for users or producers	✓	The ingredients of the materials used in this phantom are not hazardous for humans.
The product should not damage the used medical equipment, e.g. ultrasound probes	✓	The paraffin oil and thermoplastic resin in the candle gel do not interact with the medical equipment used on this phantom.
The product should contain liver parenchyma, vascularity and tumours	✘	Parenchyma and vasculature are successfully produced but the tumours that were embedded could not be located during imaging of the phantom.
The product should be patient-specific, meaning position of the mentioned anatomy must be in correspondence with the imaging it is derived from (preoperative CT or MRI)	✓	The geometry of the liver outline and vascularity was based on a preoperative model and shows accurate resemblance in terms of liver shape and vasculature layout.
The product should be 1:1 in size and volume compared to patient	✓	The volume of the final product has a negligible volume difference of 2.1%.
The product must be producible within 2 weeks	✓	The total production time of the phantom is less than 2 weeks. Model realization takes 1-2 days, 3D printing can be done simultaneously and takes approximately 3 days for the liver mold and 2 days for vasculature. Assembly of the molds, casting of the parenchyma and finishing takes 2 more days. Resulting in a total of approximately 7 days.
The product should be stable for several weeks at room temperature or in a cooled environment (7°C)	✓	The product does not suffer from microbial invasion or derogation and can be stored for at least a couple of months. Currently the phantom is stored in a water bath to prevent deformation of the liver outline and collapsing of vasculature.

5. Conclusion

The aim of this project has been to replicate a preoperative 3D model to a life size phantom. A phantom with exactly the same geometry and size of a human liver was expected to be the best simulation setting and the most suitable for development of a navigation technique.
In this thesis a method to produce a multimodal anthropomorphic liver phantom is presented. A number of material tests have been performed to select substitute materials and the assembly of a patient-specific phantom is described. From the results it can be concluded that candle gel can be used to create a phantom that produces realistic ultrasound imaging and clear intensity on MRI. The ultrasound aspect of the parenchyma substitute and vasculature have an intensity equivalent to patient scans. By comparison of the vascularity that was realized in the phantom to the vascularity that was originally segmented from the patient scan we can conclude that detailed and patient-specific vasculature can be created by means of 3D printing of Elastic resin. Once the candle gel has cooled down and solidified, the prints are extracted and a detailed cavity representing the liver vasculature remains. Compared to various commercial liver phantoms this phantom is an affordable alternative that can be reused and adjusted to meet demands of different simulation settings. For the ablation experiment a new phantom was produced that proved this custom anatomy useful. Translating the vascularity and tumours that resulted from the sample tests into the large final phantom proved to be difficult. A challenge lies in positioning tumours in the parenchyma substitute and preventing dissolving of these tumours during the production. Hence, several challenges remain in reducing vulnerability of the phantom, printing extensive prints of vasculature, permanently fill the vasculature and realizing realistic tumours. Future research should focus on producing stable tumour models that can be embedded in the desired location and protection of the phantom from damage during experiments and transportation.

6. Problems to be solved

After analysis of the results and discussing them a few recommendations can be made. The first challenge to be solved is vulnerability of the phantom. A protective cover, skin or layer is a way to protect the phantom from damage. The requirements of a protective layer are no interaction with the parenchyma material, no interference with ultrasound or MRI imaging, no major impact on probe manipulation, easy to apply and repair. Furthermore, the material should not damage imaging equipment and cannot be harmful to the user.

An option that has been tried is applying encapsulating plastic (Super Baldiez, Mouldlife Ltd., Sufflok, United Kingdom), developed to be used as a “bald cap” in special effects industry. This layer is applicable on the candle gel and is not causing problems with ultrasound. To apply this material it was thinned with Isopropyl alcohol and applied with a brush. The material should dry thoroughly for at least 2 hours. After brushing 5 layers of the material a thin layer was able to protect the phantom from damage during handling with bare hands. Because of the brushing method the edges of the liver are a vulnerable point where the layer peels off easily. When this starts to happen, water is likely to come between the protective layer and the candle gel which causes the layer to increasingly separate from the phantom.

More robust materials could improve the workability of the phantom. Vasculature imaging is nearly perfect. However, the stability and endurance of the phantom would benefit from a solid vasculature substitute that doesn’t require extraction and is not prone to collapse. A suitable material to embed directly would have the properties of minimal ultrasound reflection or absorption, to ensure the anechoic ultrasound aspect of the vasculature on ultrasound. Simultaneously, it should be rigid enough to be connected to the mold and maintain its shape when the parenchyma is cast. Another option could be filling the hollow vasculature as it is created in the phantom currently. The main problem in this approach are air bubbles that remain proximally in the vasculature or that form in the new vasculature material.

Storage is another aspect that still needs to be evaluated. The candle gel material is not vulnerable for bacterial infection or algae growth. However, when not stored properly the material will deform under the influence of gravity and its own weight. To prevent this, the phantom was kept in a water bath to prevent pressure points on the surface. The candle gel is lighter than water making the phantom float. This also prevents it from deformation as a whole. For future work the aim should be to create a permanent container that presents the phantom in the correct orientation without having to manipulate it before use. Support for the phantom could consist of a foam or gel bed molded to the back of the phantom. A universal support could be built by hanging a net or cloth to support the phantom with evenly distributed pressure without the need to fixate it in one orientation.

For use in the development of navigated ultrasound procedures the size and geometry of the phantom can be reconsidered. A downscaled or simplified model, but with adequate bifurcations can be satisfactory in the setting of surgical navigation. In a setting of practicing ultrasound guided ablation techniques, a complex vascular structure is necessary, but the liver contour can be sacrificed. Concessions on one aspect may notably increase the possibilities and feasibility of others.

References

[1] Nederlandse Kankerregistratie, “Cijfers over kanker.” [Online]. Available: https://www.cijfersoverkanker.nl/. [Accessed: 12-Nov-2019].

[2] J. Ferlay, H. R. Shin, F. Bray, D. Forman, C. Mathers, and D. M. Parkin, “Estimates of worldwide burden of cancer in 2008: GLOBOCAN 2008,” *Int. J. Cancer*, vol. 127, no. 12, pp. 2893–2917, 2010.

[3] H. B. El-Serag and A. C. Mason, “Rising incidence of hepatocellular carcinoma in the United States,” *N. Engl. J. Med.*, vol. 340, no. 10, pp. 745–750, 1999.

[4] E. Van Cutsem *et al.*, “Towards a pan-European consensus on the treatment of patients with colorectal liver metastases,” *Eur. J. Cancer*, vol. 42, no. 14, pp. 2212–2221, Sep. 2006.

[5] R. Stangl, A. Altendorf-Hofmann, R. M. Charnley, and J. Scheele, “Factors influencing the natural history of colorectal liver metastases,” *Lancet*, vol. 343, no. 8910, pp. 1405–1410, Jun. 1994.

[6] A. Jemal *et al.*, “Cancer statistics, 2005.,” *CA. Cancer J. Clin.*, vol. 55, no. 1, pp. 10–30.

[7] G. D. Leonard, B. Brenner, and N. E. Kemeny, “Neoadjuvant Chemotherapy Before Liver Resection for Patients With Unresectable Liver Metastases From Colorectal Carcinoma,” *J. Clin. Oncol.*, vol. 23, no. 9, pp. 2038–2048, Mar. 2005.

[8] R. N. Berri and E. K. Abdalla, “Curable metastatic colorectal cancer: recommended paradigms.,” *Curr. Oncol. Rep.*, vol. 11, no. 3, pp. 200–8, May 2009.

[9] U. Stein and P. M. Schlag, “Clinical, biological, and molecular aspects of metastasis in colorectal cancer.,” *Recent results in cancer research. Fortschritte der Krebsforschung. Progrès dans les recherches sur le cancer*, vol. 176. pp. 61–80, 2007.

[10] J. De Ridder, J. H. W. De Wilt, F. Simmer, L. Overbeek, V. Lemmens, and I. Nagtegaal, “Incidence and origin of histologically confirmed liver metastases: an explorative case-study of 23,154 patients,” 2016.

[11] C. Hackl, P. Neumann, M. Gerken, M. Loss, M. Klinkhammer-Schalke, and H. J. Schlitt, “Treatment of colorectal liver metastases in Germany: a ten-year population-based analysis of 5772 cases of primary colorectal adenocarcinoma,” *BMC Cancer*, vol. 14, no. 1, p. 810, Dec. 2014.

[12] M. G. House *et al.*, “Survival after Hepatic Resection for Metastatic Colorectal Cancer: Trends in Outcomes for 1,600 Patients during Two Decades at a Single Institution,” *J. Am. Coll. Surg.*, vol. 210, no. 5, pp. 744–752, May 2010.

[13] J. Figueras, C. Valls, A. Rafecas, J. Fabregat, E. Ramos, and E. Jaurrieta, “Resection rate and effect of postoperative chemotherapy on survival after surgery for colorectal liver metastases,” *Br. J. Surg.*, vol. 88, no. 7, pp. 980–985, Jul. 2001.

[14] D. J. Bentrem, R. P. Dematteo, and L. H. Blumgart, “Clinical Features of Metastatic Hepatic Malignancies View project Ampullobiliary cancer therapy View project SURGICAL THERAPY FOR METASTATIC DISEASE TO THE LIVER,” *Annu. Rev. Med*, vol. 56, pp. 139–56, 2005.

[15] R. Malafosse, C. Penna, A. Sa Cunha, and B. Nordlinger, “Surgical management of hepatic metastases from colorectal malignancies,” *Annals of Oncology*, vol. 12, no. 7. pp. 887–894,

2001.

[16] J. Scheele, R. Stang, A. Altendorf-Hofmann, and M. Paul, “Resection of colorectal liver metastases,” *World J. Surg.*, vol. 19, no. 1, pp. 59–71, 1995.

[17] P. Schlag, P. Hohenberger, and C. Herfarth, “Resection of liver metastases in colorectal cancer - competitive analysis of treatment results in synchronous versus metachronous metastases,” *Eur. J. Surg. Oncol.*, vol. 16, no. 4, pp. 360–365, 1990.

[18] C. Charnsangavej, B. Clary, Y. Fong, A. Grothey, T. M. Pawlik, and M. A. Choti, “Selection of patients for resection of hepatic colorectal metastases: Expert consensus statement,” in *Annals of Surgical Oncology*, 2006, vol. 13, no. 10, pp. 1261–1268.

[19] E. P. Misiakos, N. P. Karidis, and G. Kouraklis, “Current treatment for colorectal liver metastases,” *World J. Gastroenterol.*, vol. 17, no. 36, pp. 4067–4075, Sep. 2011.

[20] C. Couinaud, “Le Foie. Etudes anatomiques et chirurgicales. Paris 1957.” Masson & Cie.

[21] E. Lim, B. N. J. Thomson, S. Heinze, M. Chao, D. Gunawardana, and P. Gibbs, “Optimizing the approach to patients with potentially resectable liver metastases from colorectal cancer,” *ANZ Journal of Surgery*, vol. 77, no. 11. pp. 941–947, 2007.

[22] D. Zorzi *et al.*, “Comparison between hepatic wedge resection and anatomic resection for colorectal liver metastases,” in *Journal of Gastrointestinal Surgery*, 2006, vol. 10, no. 1, pp. 86–94.

[23] S. Vadera and J. Jones, “Couinaud classification of hepatic segments.” [Online]. Available: https://radiopaedia.org/cases/hepatectomy-and-sectionectomy-diagrams?lang=us. [Accessed: 13-Nov-2019].

[24] G. Garcea, T. D. Lloyd, C. Aylott, G. Maddern, and D. P. Berry, “The emergent role of focal liver ablation techniques in the treatment of primary and secondary liver tumours,” *Eur. J. Cancer*, vol. 39, no. 15, pp. 2150–2164, 2003.

[25] K. Tabuse, “A new operative procedure of hepatic surgery using a microwave tissue coagulator,” *Arch. fur Japanische Chir.*, vol. 48, no. 2, pp. 160–172, 1979.

[26] C. Correa-Gallego *et al.*, “A Retrospective Comparison of Microwave Ablation vs. Radiofrequency Ablation for Colorectal Cancer Hepatic Metastases,” *Oncol*, vol. 21, pp. 4278–4283, 2014.

[27] S. Bipat *et al.*, “Colorectal liver metastases: CT, MR imaging, and PET for diagnosis - Meta-analysis,” *Radiology*, vol. 237, no. 1, pp. 123–131, 2005.

[28] H. S. Hochster *et al.*, “Safety and efficacy of oxaliplatin and fluoropyrimidine regimens with or without bevacizumab as first-line treatment of metastatic colorectal cancer: Results of the TREE study,” *J. Clin. Oncol.*, vol. 26, no. 21, pp. 3523–3529, 2008.

[29] C. Tournigand *et al.*, “FOLFIRI followed by FOLFOX6 or the reverse sequence in advanced colorectal cancer: A randomized GERCOR study,” *J. Clin. Oncol.*, vol. 22, no. 2, pp. 229–237, 2004.

[30] J. Y. Douillard *et al.*, “Irinotecan combined with fluorouracil compared with fluorouracil alone. as first-line treatment for metastatic colorectal cancer: a multicentre randomised trial,” *Lancet*, vol. 355, no. 9209, pp. 1041–1047, 2000.

[31] G. Hocking, S. Hebard, and C. H. Mitchell, “A review of the benefits and pitfalls of phantoms in ultrasound-guided regional anesthesia,” *Regional Anesthesia and Pain Medicine*, vol. 36, no. 2. pp. 162–170, 2011.

[32] A. de Gramont *et al.*, “Randomized trial comparing monthly low-dose leucovorin and fluorouracil bolus with bimonthly high-dose leucovorin and fluorouracil bolus plus continuous infusion for advanced colorectal cancer: A French intergroup study,” *J. Clin. Oncol.*, vol. 15, no. 2, pp. 808–815, 1997.

[33] M. G. van Vledder, M. C. de Jong, T. M. Pawlik, R. D. Schulick, L. A. Diaz, and M. A. Choti, “Disappearing Colorectal Liver Metastases after Chemotherapy: Should we be Concerned?,” *J. Gastrointest. Surg.*, vol. 14, no. 11, pp. 1691–1700, 2010.

[34] R. C. Auer *et al.*, “Predictors of a true complete response among disappearing liver metastases from colorectal cancer after chemotherapy,” *Cancer*, vol. 116, no. 6, pp. 1502–1509, 2010.

[35] A. Ferrero, S. Langella, N. Russolillo, L. Vigano, R. Lo Tesoriere, and L. Capussotti, “Intraoperative Detection of Disappearing Colorectal Liver Metastases as a Predictor of Residual Disease.”

[36] S. Benoist *et al.*, “Complete response of colorectal liver metastases after chemotherapy: does it mean cure?,” *J. Clin. Oncol.*, vol. 24, no. 24, pp. 3939–45, Aug. 2006.

[37] D. Elias *et al.*, “Evolution of Missing Colorectal Liver Metastases Following Inductive Chemotherapy and Hepatectomy,” *J. Surg. Oncol.*, vol. 86, no. 1, pp. 4–9, 2004.

[38] O. Heizmann *et al.*, “Assessment of intraoperative liver deformation during hepatic resection: Prospective clinical study,” *World J. Surg.*, vol. 34, no. 8, pp. 1887–1893, 2010.

[39] S. Beller, M. Hünerbein, T. Lange, S. Eulenstein, B. Gebauer, and P. M. Schlag, “Image-guided surgery of liver metastases by three-dimensional ultrasound-based optoelectronic navigation,” *Br. J. Surg.*, vol. 94, no. 7, pp. 866–875, 2007.

[40] T. Lange *et al.*, “3D ultrasound-CT registration of the liver using combined landmark-intensity information,” *Int. J. Comput. Assist. Radiol. Surg.*, vol. 4, no. 1, pp. 79–88, 2009.

[41] G. Hoch, V. Croise-Laurent, A. Germain, L. Brunaud, L. Bresler, and A. Ayav, “Is intraoperative ultrasound still useful for the detection of colorectal cancer liver metastases?,” *HPB*, vol. 17, no. 6, pp. 514–519, Jun. 2015.

[42] C. J. Harvey and T. Albrecht, “Ultrasound of focal liver lesions,” *Eur. Radiol.*, vol. 11, no. 9, pp. 1578–1593, 2001.

[43] M. M. Schonland, G. H. Millward-Sadler, D. H. Wright, and R. Wright, “Hepatic tumours,” *Liver biliary Dis.*, p. 897, 1979.

[44] K. Wernecke, P. Vassallo, U. Bick, S. Diederich, and P. E. Peters, “The distinction between benign and malignant liver tumors on sonography: Value of a hypoechoic halo,” *Am. J. Roentgenol.*, vol. 159, no. 5, pp. 1005–1009, 1992.

[45] A. P. Dhawan, *Medical Image Analysis: Second Edition*. 2010.

[46] M. W. Bowyer and R. B. Fransman, “Simulation in General Surgery,” 2019, pp. 171–183.

[47] M. A. Malangoni, T. W. Biester, A. T. Jones, M. E. Klingensmith, and F. R. Lewis, “Operative experience of surgery residents: Trends and challenges,” in *Journal of Surgical Education*,

2013, vol. 70, no. 6, pp. 783–788.

[48] A. L. Fonseca, L. V. Evans, and R. J. Gusberg, “Open surgical simulation in residency training: A review of its status and a case for its incorporation,” *J. Surg. Educ.*, vol. 70, no. 1, pp. 129–137, 2013.

[49] M. O. Culjat, D. Goldenberg, P. Tewari, and R. S. Singh, “A review of tissue substitutes for ultrasound imaging,” *Ultrasound in Medicine and Biology*, vol. 36, no. 6. pp. 861–873, 2010.

[50] S. L. Vieira, T. Z. Pavan, J. E. Junior, and A. A. O. Carneiro, “Paraffin-Gel Tissue-Mimicking Material for Ultrasound-Guided Needle Biopsy Phantom,” *Ultrasound Med. Biol.*, vol. 39, no. 12, pp. 2477–2484, 2013.

[51] N. Shevchenko, J. Schwaiger, M. Markert, W. Flatz, and T. C. Lueth, “Evaluation of a resectable ultrasound liver phantom for testing of surgical navigation systems,” in *Proceedings of the Annual International Conference of the IEEE Engineering in Medicine and Biology Society, EMBS*, 2011, pp. 916–919.

[52] K. Zell, J. I. Sperl, M. W. Vogel, R. Niessner, and C. Haisch, “Acoustical properties of selected tissue phantom materials for ultrasound imaging,” *Phys. Med. Biol.*, vol. 52, no. 20, 2007.

[53] T. Kondo, M. Kitatuji, Y. Shikinami, K. Tuta, and H. Kanda, “New tissue mimicking materials for ultrasound phantoms,” in *Proceedings - IEEE Ultrasonics Symposium*, 2005, vol. 3, pp. 1664–1667.

[54] A. Rethy *et al.*, “Anthropomorphic liver phantom with flow for multimodal image-guided liver therapy research and training,” *Int. J. Comput. Assist. Radiol. Surg.*, vol. 13, no. 1, pp. 61–72, 2018.

[55] A. Kharine *et al.*, “Poly(vinyl alcohol) gels for use as tissue phantoms in photoacoustic mammography,” *Phys. Med. Biol.*, vol. 48, no. 3, pp. 357–370, 2003.

[56] M. Carbone, S. Condino, L. Mattei, P. Forte, V. Ferrari, and F. Mosca, “Anthropomorphic ultrasound elastography phantoms Characterization of silicone materials to build breast elastography phantoms,” in *Proceedings of the Annual International Conference of the IEEE Engineering in Medicine and Biology Society, EMBS*, 2012, vol. 2012, pp. 492–494.

[57] L. E. Maggi, M. A. Von Krüger, W. C. A. Pereira, and E. E. C. Monteiro, “Development of silicon-based materials for ultrasound biological phantoms,” in *Proceedings - IEEE Ultrasonics Symposium*, 2009.

[58] A. Pacioni, M. Carbone, C. Freschi, R. Viglialoro, V. Ferrari, and M. Ferrari, “Patient-specific ultrasound liver phantom: materials and fabrication method,” *Int. J. Comput. Assist. Radiol. Surg.*, vol. 10, no. 7, pp. 1065–1075, 2015.

[59] M. M. Burlew, E. L. Madsen, J. A. Zagzebski, R. A. Banjavic, and S. W. Sum, “A new ultrasound tissue-equivalent material.,” *Radiology*, vol. 134, no. 2, pp. 517–20, Feb. 1980.

[60] N. L. Bush and C. R. Hill, “Gelatine-alginate complex gel: a new acoustically tissue-equivalent material.,” *Ultrasound Med. Biol.*, vol. 9, no. 5, pp. 479–84, Sep. 1983.

[61] I. Miller De Carvalho *et al.*, “Polyvinyl chloride plastisol breast phantoms for ultrasound imaging,” *Ultrasonics*, vol. 70, pp. 98–106, 2016.

[62] G. M. Spirou, A. A. Oraevsky, I. Alex Vitkin, and W. M. Whelan, “Optical and acoustic

properties at 1064 nm of polyvinyl chloride-plastisol for use as a tissue phantom in biomedical optoacoustics," *Phys. Med. Biol.*, vol. 50, no. 14, pp. 141–153, 2005.

[63] K. J. M. Surry, H. J. B. Austin, A. Fenster, and T. M. Peters, "Poly(vinyl alcohol) cryogel phantoms for use in ultrasound and MR imaging," *Phys. Med. Biol.*, vol. 49, no. 24, pp. 5529–5546, 2004.

[64] A. Nava, E. Mazza, M. Furrer, P. Villiger, and W. H. Reinhart, "In vivo mechanical characterization of human liver," *Med. Image Anal.*, vol. 12, no. 2, pp. 203–216, Apr. 2008.

[65] T. J. Hall, M. Bilgen, M. F. Insana, and T. A. Krouskop, "Phantom Materials for Elastography," 1997.

[66] J. Schwaiger, M. Markert, N. Shevchenko, and T. C. Lueth, "The effects of real-time image navigation in operative liver surgery," *Int. J. Comput. Assist. Radiol. Surg.*, vol. 6, no. 6, pp. 785–796, 2011.

[67] N. Hungr, J. A. Long, V. Beix, and J. Troccaz, "A realistic deformable prostate phantom for multimodal imaging and needle-insertion procedures," *Med. Phys.*, vol. 39, no. 4, pp. 2031–2041, 2012.

[68] B. Sen Chiou and P. E. Schoen, "Effects of crosslinking on thermal and mechanical properties of polyurethanes," *J. Appl. Polym. Sci.*, vol. 83, no. 1, pp. 212–223, 2002.

[69] G. M. Bernacca, B. O'Connor, D. F. Williams, and D. J. Wheatley, "Hydrodynamic function of polyurethane prosthetic heart valves: Influences of Young's modulus and leaflet thickness," *Biomaterials*, vol. 23, no. 1, pp. 45–50, 2002.

[70] Smooth-On Inc, "VytaFlex 10." 2019.

[71] J. Fromageau, J.-L. Gennisson, C. Schmitt, R. L. Maurice, R. Mongrain, and G. Cloutier, "Estimation of polyvinyl alcohol cryogel mechanical properties with four ultrasound elastography methods and comparison with gold standard testings," *IEEE Trans. Ultrason. Ferroelectr. Freq. Control*, vol. 54, no. 3, pp. 498–509, Mar. 2007.

[72] Smooth-On Inc, "EcoFlex 00-10." 2019.

[73] M. K. Chmarra, R. Hansen, R. Mårvik, and T. Langø, "Multimodal Phantom of Liver Tissue," *PLoS One*, vol. 8, no. 5, 2013.

[74] Matterhackers.com, "PORO-LAY GEL-LAY Porous Filament - 1.75mm (0.25kg)," 2019. [Online]. Available: https://www.matterhackers.com/store/3d-printer-filament/poro-lay-gel-lay-porous-filament-175mm. [Accessed: 11-May-2019].

[75] Formlabs Inc., "Material Datasheet: Elastic Resin," pp. 1–2, 2019.

[76] M. Thielen, "ReVive: designing the newborn life support manikin," Technische Universiteit Eindhoven, 2019.

[77] S. L. Vieira, T. Z. Pavan, J. E. Junior, and A. A. O. Carneiro, "Paraffin-Gel Tissue-Mimicking Material for Ultrasound-Guided Needle Biopsy Phantom," *Ultrasound Med. Biol.*, vol. 39, no. 12, pp. 2477–2484, 2013.

[78] P. Reimer, G. Schneider, and W. Schima, "Hepatobiliary contrast agents for contrast-enhanced MRI of the liver: Properties, clinical development and applications," *European Radiology*, vol. 14, no. 4. pp. 559–578, 2004.

[79] A. Fedorov *et al.*, “3D Slicer as an image computing platform for the Quantitative Imaging Network.,” *Magn. Reson. Imaging*, vol. 30, no. 9, pp. 1323–41, Nov. 2012.

[80] O. Ivashchenko, E.-J. Rijkhorst, and L. ter Beek, “Automated segmentation of the liver and hepatic vasculature, and biliary tree anatomy from multiphase MR images,” *Magn. Reson. Imaging*, 2019.

[81] T. Heimann *et al.*, “Comparison and evaluation of methods for liver segmentation from CT datasets,” *IEEE Trans. Med. Imaging*, vol. 28, no. 8, pp. 1251–1265, 2009.

[82] G. Litjens *et al.*, “Evaluation of prostate segmentation algorithms for MRI: The PROMISE12 challenge,” *Med. Image Anal.*, 2014.

[83] L. W. Clements, W. C. Chapman, B. M. Dawant, R. L. Galloway, and M. I. Miga, “Robust surface registration using salient anatomical features for image-guided liver surgery: Algorithm and validation,” *Med. Phys.*, vol. 35, no. 6, pp. 2528–2540, 2008.

Appendix A

The materials that were tested in the material selection have been used in a study on dosimetry optimization of CT protocols. All produced material samples were imaged using different CT tube voltage settings to analyze Hounsfield units (HUs) and compare them to the average human soft tissue HUs. A custom polyurethane rubber mix was found to be an accurate soft tissue substitute in CT and was used to build two arm phantoms. These arms, attached to the RANDO phantom are used to optimize CT protocols with complex arm positions.

The abstract written below was submitted to, and accepted for the European Congress of Radiology (ECR) and will be presented on March 11, 2020 8:30-10:00 in Vienna.

Development of an articulated anthropomorphic 3D-printed arm phantom for image quality and dosimetry optimization of CT protocols

Ivashchenko OV[1], Ruitenbeek HC[2,3], Boonekamp M[4], Fusaglia M[2], Hernandez-Giron I[1]

[1]Department of Radiology, Leiden University Medical Center, Albinusdreef 2, 2333ZA, Leiden, The Netherlands.

[2]Surgical Oncology, The Netherlands Cancer Institute – Antoni van Leeuwenhoek Hospital, Plesmanlaan 121, 1066 CX, Amsterdam, The Netherlands.

[3]Technical medicine, University of Twente, Drinerlolaan 5, 7522 NB, Enschede, The Netherlands

[4]Department of Research and Development, Leiden University Medical Center, Albinusdreef 2, 2333ZA, Leiden, The Netherlands.

Purpose:

To guarantee optimal diagnostic image quality-to-dose trade-off in CT, acquisition and reconstruction parameters are optimized for standardized patient positions. For indications related to anatomical regions between lower abdomen and up to the head, arms should be placed outside the field-of-view. However, for a large group of patients, including trauma or restricted shoulder mobility cases, one or both arms can be fully immobilized. Then, arm-positioning-specific instructions do not apply, affecting dose and image quality. This could be overcome using trauma-specific CT protocols adapted for nontrivial arm positions. CT-manufacturers allow for complex dose modulation with nontrivial arm-positioning, but implementation and optimization in clinical practice is rare. One of the reasons is the scarcity of commercially available phantoms for CT-dosimetry with articulated arms. Our goal was to develop affordable and reproducible production methods of totally articulated arm extensions of a RANDO-phantom, widely used for CT quality control in Radiology and Radiotherapy.

Methods and Materials:

3D-modelling, 3D-printing and molding techniques were used to manufacture the phantom, using anthropomorphic bones and soft-tissue-like materials. After testing various 3D-printing, silicone, gels and polyurethane materials, a nylon-aluminum mix alumide and a custom polyurethane-rubber mix were selected, corresponding to average HUs of human hard bone and fat-muscle mix, respectively. Image quality, attenuation, and dose modulation properties of the phantom, attached to RANDO-phantom, were evaluated for trauma-CT protocols.

Results:

Attenuation of the phantom [bone:(562±336)HU, soft_tissue:(56±24)HU] closely mimicked values of the human arm [compact-bone:(800±400)HU, fat-to-muscle:(-80:100)HU], and is stable within 80-140kV range. CTDIvol dose of the thorax trauma-CT varied by 12% (0.3 mGy) for various arm positions (arms-up, down and mixed).

Conclusion:

A reproducible method for production of totally-articulated arm phantom for CT-imaging was developed, to optimize new CT protocols with complex arm positions.

Keywords: radiation dose, thorax CT, liver CT, anthropomorphic phantom.

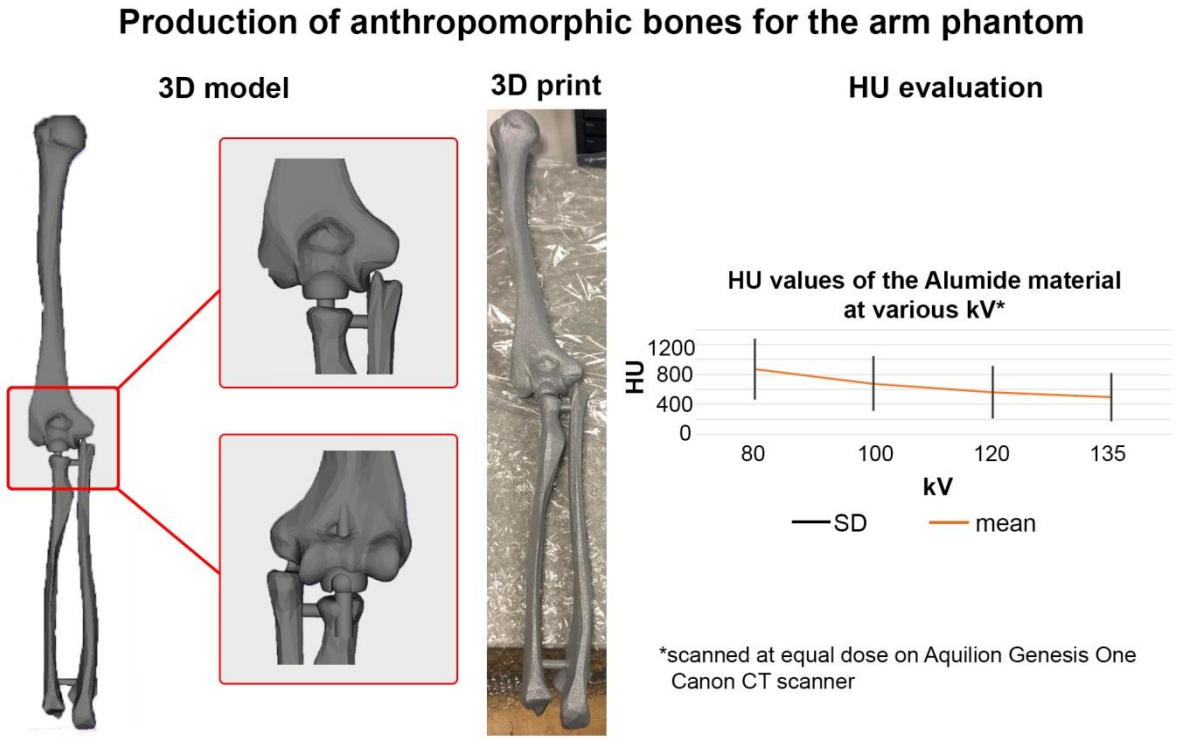

Selection of soft tissue matarials

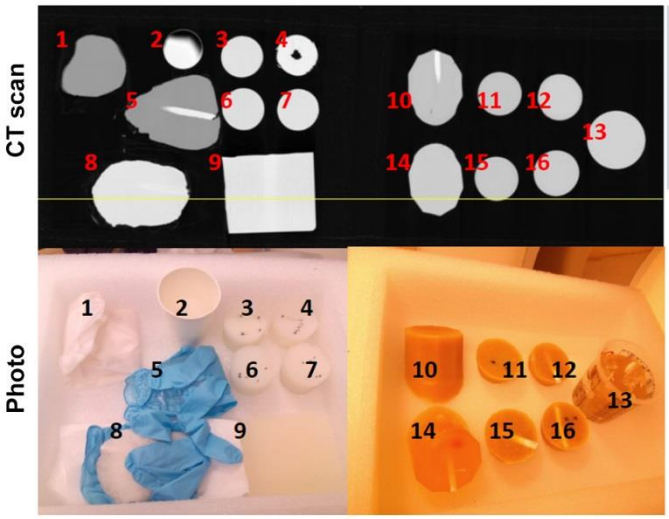

List of materials:

1. Candel gel # 2*
2. Silicone # 1*
3. Silicone # 4*
4. Silicone # 7*
5. Candle gel # 1*
6. Silicone # 5*
7. Silicone # 6*
8. Silicone # 2*
9. Silicone # 3*
10. Polyurethane
11. Polyurethane rubber (PR) # 2*
12. PR # 4*
13. PR # 5*
14. Plastisole
15. PR # 1*
16. PR # 3* - selected for the phantom

**custom mix*

HU unit of soft materials at various kV

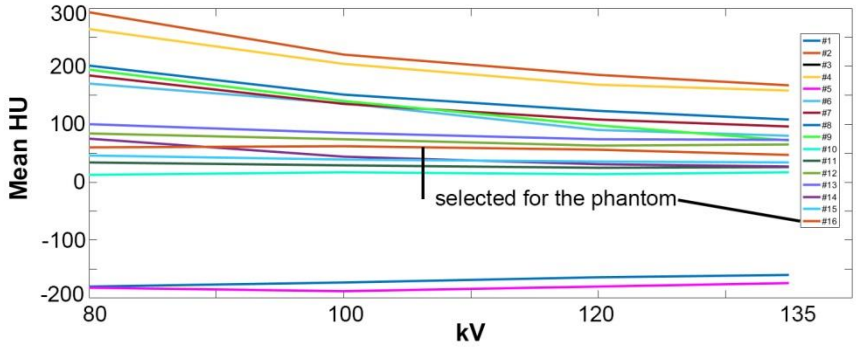

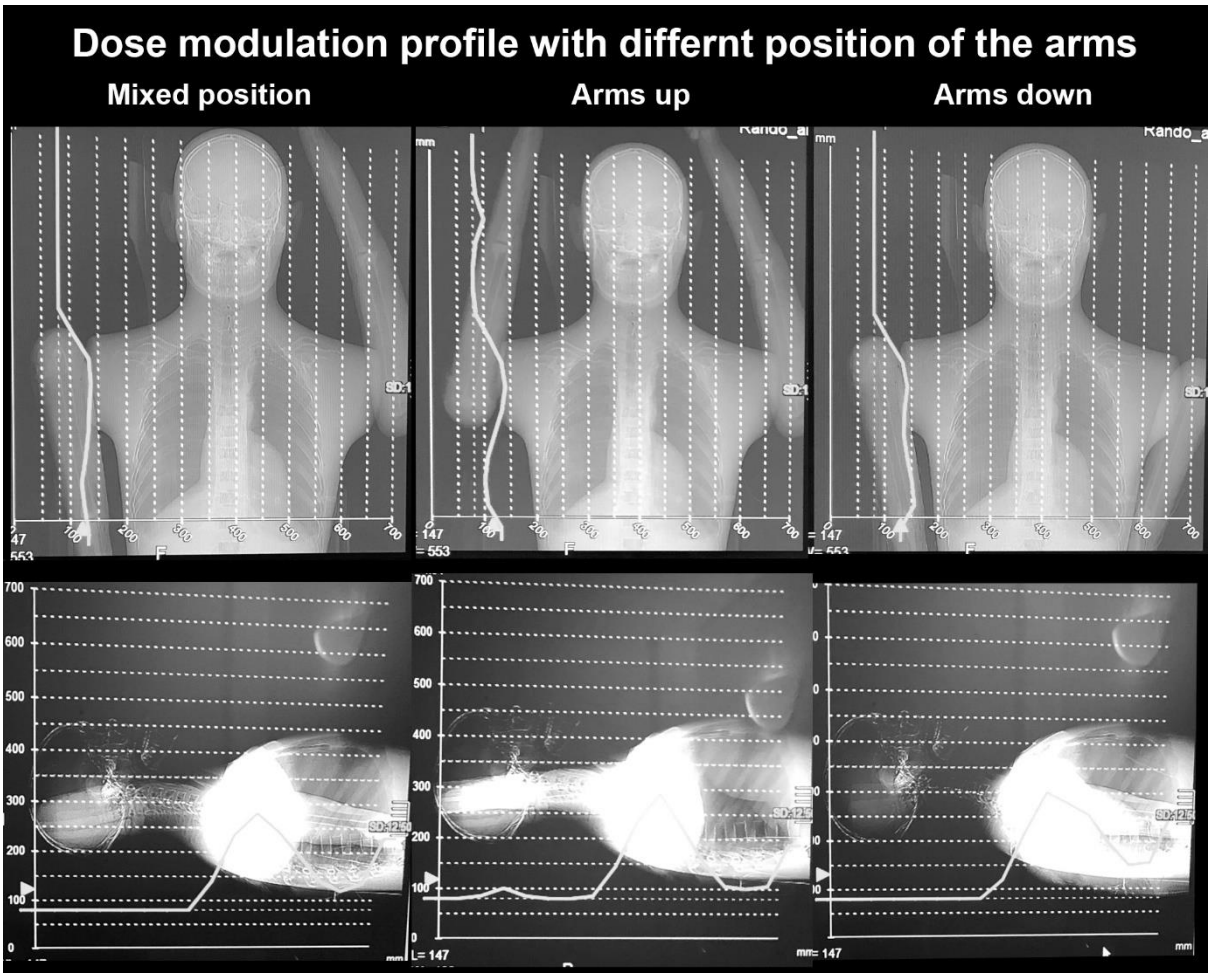
Dose modulation profile with differnt position of the arms
Mixed position
Arms up
Arms down